Impact of Stereochemical Replacement on the Activity and Selectivity of Membrane-Active Cationic Cyclic Peptides with Broad-Spectrum Antibacterial and Antifungal Activity

Sandeep Lohan,[§,$] Anastasia G. Konshina,[‡] Eman H.M. Mohammed,[§,σ] Naiera M. Helmy,[§,Ω] Srishhti K. Jha,[†] Rakesh Kumar Tiwari,[§,ϑ] Innokentiy Maslennikov,[†] Roman G. Efremov,[‡,§,] Keykavous Parang[§,*]

[§]Center for Targeted Drug Delivery, Department of Biomedical and Pharmaceutical Sciences, Chapman University School of Pharmacy, Harry and Diane Rinker Health Science Campus, 9401 Jeronimo Rd, Irvine, California 92618, United States

[$]AJK Biopharmaceutical, 5270 California Ave, Irvine, CA 92617

[†]Structural Biology Research Center, Department of Biomedical and Pharmaceutical Sciences, Chapman University School of Pharmacy, Harry and Diane Rinker Health Science Campus, 9401 Jeronimo Rd., Irvine, California 92618, United States

[σ]Chemistry Department, Faculty of Science, Menoufia University, Shebin El-Koam, 51132, Egypt

[Ω]Microbial Biotechnology Department, Biotechnology Research Institute, National Research Centre, Giza, Egypt

[ϑ]Department of Biomedical Sciences, College of Osteopathic Medicine of the Pacific-Northwest, Western University of Health Sciences, Lebanon, OR 97355, USA

[‡]M.M. Shemyakin & Yu.A. Ovchinnikov Institute of Bioorganic Chemistry, Russian Academy of Sciences, Miklukho-Maklaya Street, 16/10, Moscow, 117997, Russia

[§]National Research University Higher School of Economics, Myasnitskaya ul. 20, Moscow, 101000, Russia

Abstract

Herein, we report a library of 7-mer macrocyclic peptides designed by systematically replacing one, multiple, or all L-amino acids with their D-isomers in our previously identified hit compounds. Lead peptides, **15c** and **16c**, showed broad-spectrum activity against bacteria (Gram-positive minimum inhibitory activity (MIC 1.5-6.2 µg/mL and Gram-negative MIC 6.2-25 µg/mL), and fungi (MIC = 3.1-25 µg/mL). Additionally, peptides **15c** and **16c** showed rapid kill kinetics and biofilm degradation potential against both bacteria and fungi, while resistance development was not observed. The antimicrobial effect of these macrocyclic peptides was attributed to their membranolytic action, which was confirmed by calcein dye leakage assay and scanning electron microscopy analysis. Both peptides, **15c** (HC_{50} = 335 µg/mL) and **16c** (HC_{50} = 310 µg/mL), exhibited significantly lower hemolytic activity compared to their parent peptide **p3** (HC_{50} = 230 µg/mL). At 100 µg/mL, both peptides showed > 90% cell viability after 24 h incubation across four normal mammalian cell lines. Both peptides showed plasma stability ($t_{1/2} \geq$ 6h), further supporting their therapeutic potential. Finally, the molecular mechanisms determining the pharmacological properties of a number of typical representatives of each series of synthesized peptides were investigated by NMR spectroscopy and computer simulations. The study revealed specific combinations of structural, dynamic, and hydrophobic parameters of these amphiphilic peptides that allow a reasonable prediction of their hemolytic activity. This Structure-Activity Relationship provides a basis for the rational design of peptides or peptidomimetics with predefined pharmacological profiles.

Keywords: Amphipathicity; Antifungal; Antimicrobial; Macrocyclic; Membranolytic Action; Molecular Hydrophobicity Potential; Molecular Simulations; NMR; Peptides; Surface Hydrophobic Pattern.

1. INTRODUCTION

The emergence of antibiotic resistance poses a significant challenge to modern medicine and global healthcare systems. Infections caused by resistant pathogens now result in higher morbidity and mortality rates, longer hospital stays, and increased treatment costs, placing a greater burden on healthcare resources.[1, 2] According to the 2019 U.S. Center For Disease Control (CDC) report, antibiotic resistance in the United States has been on the rise, with 2.8 million infections and more than 35,000 deaths annually.[3, 4] Hence, these trends highlight the pressing need for new antimicrobial agents that are less prone to resistance than conventional antibiotics.

Since the identification of the first antimicrobial peptide (AMP), cecropin, from silk moths (*Hyalophora cecropia*) in the early 1980s, approximately 2000 AMPs, have been isolated from various biological sources from insects to humans.[5-7] The unique therapeutic features of AMPs, such as nonspecific mode of action and broad-spectrum activity, have attracted the attention of many research groups around the world.[8, 9] Many reports have proposed that AMPs exert their action by binding to the cell membrane, causing cell death by direct membrane disruption or translocation into the cytosol where potential internal targets are affected.[9-11] AMPs are known to exert microbial killing via a unique, multifaceted mode of action, which makes it very difficult for pathogens to develop resistance against them.[12] In addition, the different mode of action of AMPs compared to the conventional antibiotics, which specifically target cellular components at various levels, explains their broad spectrum of activity, including against drug-resistant pathogens.[13-15] Consequently, extensive efforts have been made to develop AMPs as novel antimicrobial agents.[16-18] In addition to the native lipo- and glycopeptide antibiotics such as daptomycin, polymyxin B, and vancomycin, which are already available on the market, many synthetic AMPs are still in the drug development phase, yet to reach clinical application.[18-20] Despite being recognized as a promising class of molecules for many years, AMPs have not made a substantial impact in the treatment of infections caused by resistant bacteria and fungi. This limitation is mainly due to clinical challenges, such as cytotoxicity and poor pharmacokinetics associated with AMPs, mainly attributed to their comparatively large molecular size and susceptibility to protease degradation.[18, 20]

The past two decades have witnessed the emergence of macrocycles, including macrocyclic peptides, as a promising yet underexploited class of de novo drug candidates.[21, 22] Macrocyclic molecules represent a unique chemical class, with features such as structural compactness and high stability against enzymatic degradation, making them highly suitable for

drug development.[22, 23] The therapeutic potential of macrocycles is further evident from the discovery of various naturally occurring peptides-based anti-infectives, such as daptomycin, polymyxin B, vancomycin, amphotericin B, and gramicidin S, all of which possess a well-defined cyclic structural framework.[24, 25] Accordingly, over the years, to address the clinical drawbacks associated with AMPs, numerous chemical modification strategies have been implemented to devise macrocyclic molecules with structural rigidity and enzymatic stability.[22, 23, 25] Previous studies have revealed the importance of the orientation of the side chain functionalities in facilitating effective electrostatic and/or hydrophobic interactions with target membranes.[26-28] Thus, backbone stereochemistry could greatly influence the membrane interaction properties of peptide molecules.

We have developed small synthetic cyclic amphiphilic AMPs and have reported a series of cationic macrocyclic peptides composed of various natural and unnatural amino acid residues, demonstrating promising antibacterial activity as well as high enzymatic stability.[29-32] Our previous investigations explored the number and respective positions of cationic and hydrophobic residues, providing valuable insights into structure-activity relationships (SAR) in cyclic peptides and offering guidance for designing novel macrocyclic scaffolds with favorable structural properties.[29, 30, 32]

In this study, to further improve key therapeutic properties in addition to efficacy, such as selectivity and stability, we are reporting a new series of cyclic peptides designed by systematically replacing the cationic and/or hydrophobic residues with their respective D-isomers. All synthesized cyclic peptides were screened against a wide range of Gram-positive and Gram-negative bacteria and fungi, including drug-resistant strains. *In vitro* cytotoxicity of the peptides was evaluated by measuring the cell viability against different types of normal mammalian cells and lytic activity against human red blood cells (hRBCs). The bactericidal and fungicidal kinetics and biofilm disruption potential of the lead cyclic peptides were measured and compared with the standard antibiotics. The proteolytic stability and potential of lead cyclic peptides against resistant and non-resistant bacteria were determined. We also examined the membrane perturbation action of the lead peptides by conducting calcein dye leakage assay, with further confirmation by scanning electron microscopy (SEM). A detailed analysis of structural, dynamic, and hydrophobic properties of lead cyclic peptides was conducted using Nuclear Magnetic Resonance (NMR) spectroscopy and molecular modeling in aqueous solution and in water-lipid environments that mimic bacterial and mammalian membranes. Altogether, the activity results of the lead cyclic peptide, along with the interaction

studies in the presence of model phospholipid bilayer membranes, provided insight into the peptides' membrane disruptive mechanism.

2. RESULTS AND DISCUSSION

2.1. Design and synthesis

Most naturally occurring and synthetically designed AMPs have been found to exert their antimicrobial activity via membrane disruption.[12-15] Therefore, for macrocyclic peptides, in addition to key physicochemical properties such as net cationic charge, hydrophobic bulk, ring size, and backbone flexibility, the special orientation of the side chain could play a crucial role in selective and effective membrane interaction properties of macrocyclic peptides towards target microbial membranes.

We envisioned that a systematic stereochemical substitution among the molecules, with fixed numbers and positions of the cationic and hydrophobic residues, could favorably orient the side chains, particularly by fine-tuning the hydrophobic bulk through the packing pattern of hydrophobic side chains. In addition, peptides composed of D-amino acids tend to have higher stability against peptidases.[33]

Building on our previously identified lead molecules (**p1**: c[Arg-Arg-Arg-Arg-Dip-Dip-Dip], **p2**: c[Arg-Arg-Arg-Arg-Nal-Nal-Nal][30], **p3**: c[Arg-Arg-Arg-Arg-Dip-Trp-Dip], **p4**: c[Arg-Arg-Arg-Arg-Nal-Trp-Nal], **p5**: c[Arg-Arg-Arg-Arg-Trp-Nal-Nal][32]), we designed five distinct series of cyclic amphiphilic peptides by systematically replacing cationic and hydrophobic residues with their respective stereoisomers. Series 1 (**1a**-**16a**), Series 2 (**1b**-**16b**), Series 3 (**1c**-**24c**), Series 4 (**1d**-**24d**), and Series 5 (**1e**-**11e**) were designed using the peptide sequence p1, p2, p3, p4, and p5 as templates, respectively (Scheme 1). In Series 1 through Series 4, we focused on determining the impact of stereochemical replacement ("L" to "D") of individual amino acid residues. The initial set of molecules (**1a**-**7a**, **1b**-**7b**, **1c**-**7c**, and **1d**-**7d**) were designed by substituting one L- amino acid residue at a time with its D- isomer. To further investigate the effect of stereoisomeric substitutions, we designed peptides by introducing D-enantiomers of all residues (**8a**, **8b**, **8c**, **8d**, and **1e**) or all hydrophobic residues (**11a**, **12a**, **15a**, **16a**, **11b**, **12b**, **15b**, **16b**, **10c**, **17c**-**20c**, **10d**, **17d**-**20d**, **3e**, **8e** and **9e**), or all cationic residues (**10a**, **10b**, **9c**, **12c**, **9d**, **12d**, and **2e**), as well as substitutions of multiple residues at alternate or adjacent positions (**11a**-**16a**, **11b**-**16b**, **11c**-**24c**, **11d**-**24d**, and **4e**-**11e**) (Scheme 1).

All peptides were synthesized using standard Fmoc/tBu solid-phase chemistry. After assembling the desired peptide sequences, fully protected linear peptides were obtained by

cleavage of the peptidyl resin in mildly acidic conditions while protecting the side-chain protecting groups. Fully protected linear peptides were subjected to head-to-tail cyclization in the presence of activation and coupling reagents, followed by complete deprotection resulting in cyclized peptides, as described in the experimental section. All the synthesized cyclic peptides were purified using reverse-phase high-performance liquid chromatography (HPLC) and were found to be >95% pure. High-resolution mass spectrometry (HR-MS) data were obtained in ESI mode. These results confirm the structure of the synthesized peptides. The HPLC purity and HR-MS data of all cyclic peptides have been provided in the supporting information.

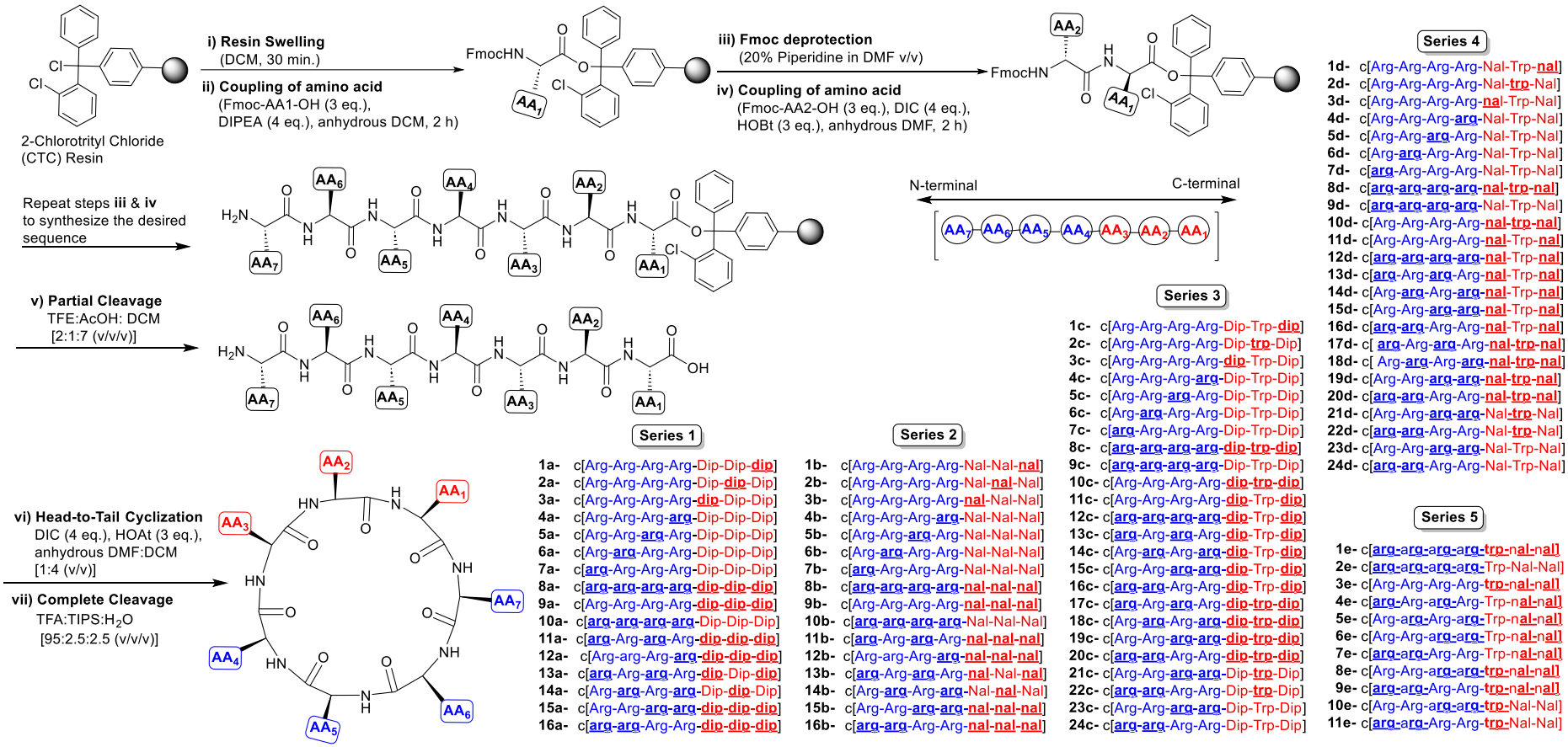

Scheme 1. Overview of the steps involved in the solid phase synthesis of cyclic peptides. Amino acid residues are represented in three-letter notation: Arg, L-arginine; Trp, L-tryptophan; Dip, 3,3-diphenyl-L-alanine; Nal, 3-(2-naphthyl)-L-alanine. D-amino acids, **arg**, **trp**, **dip**, and **nal** are indicated in bold font with an underline. Cationic and hydrophobic residues are depicted in blue and red color, respectively.

2.2. Antimicrobial activity

2.2.1. Antibacterial activity

The antibacterial activity of all the synthesized cyclic peptides was determined against a wide range of Gram-positive and Gram-negative bacteria, including their antibiotic-resistant strains. The results of all the tested cyclic peptides against Gram-positive bacteria are presented in the form of a heatmap, Figure 1A (Table S3, supporting information).

All cyclic peptides displayed antibacterial activity against *S. aureus*, *E. faecium*, *B. subtilis*, and *B. cereus*, with minimum inhibitory concentrations (MICs) in the range of 1.5-6.2 µg/mL. Notably, most of the cyclic peptides showed similar activities against the antibiotic-resistant strains of *S. aureus* and *E. faecium*. Compared to *E. faecium*, most of the cyclic peptides showed slightly reduced activity against both wild type (MIC = 3.1-12.5 µg/mL) and vancomycin-resistant (MIC = 6.2-12.5 µg/mL) *E. faecalis*. Interestingly, while all cyclic peptides displayed moderate activity against wild-type *S. pneumoniae* (MIC = 25-50 µg/mL), most of the cyclic peptides showed 1 to 2-fold higher activity against antibiotic-resistant *S. pneumoniae* (MIC = 12.5-25 µg/mL). Compared to standard antibiotic daptomycin, most of the cyclic peptides showed comparable or higher activity against vancomycin-resistant strains of *E. faecium* and *E. faecalis* (Table S3, Supporting Information).

Compared to their activity against Gram-positive bacteria, all cyclic peptides displayed reduced potency against the tested gram-negative strains (Figure 1A and Table S4 Supporting Information). All cyclic peptides showed moderate activity against both wild-type and resistant strains of *E. coli* with MICs in the range of 6.2-25 µg/mL. For all tested cyclic peptides, a similar trend of activity was observed against the ciprofloxacin-resistant *A. baumannii* (MIC = 6.2-25 µg/mL). However, slightly lower activity was observed against both wild-type and imipenem-resistant *P. aeruginosa* (MIC = 12.5-50 µg/mL). Among all tested Gram-negative bacterial strains, most cyclic peptides showed the weakest activity against *K. pneumonia* strains. However, when compared to wild-type *K. pneumonia* (MIC = 50->50 µg/mL), most of the cyclic peptides displayed enhanced activity against carbapenem-resistant *K. pneumonia* (MIC = 12.5->50 µg/mL; Figure 1A and Table S4 Supporting Information).

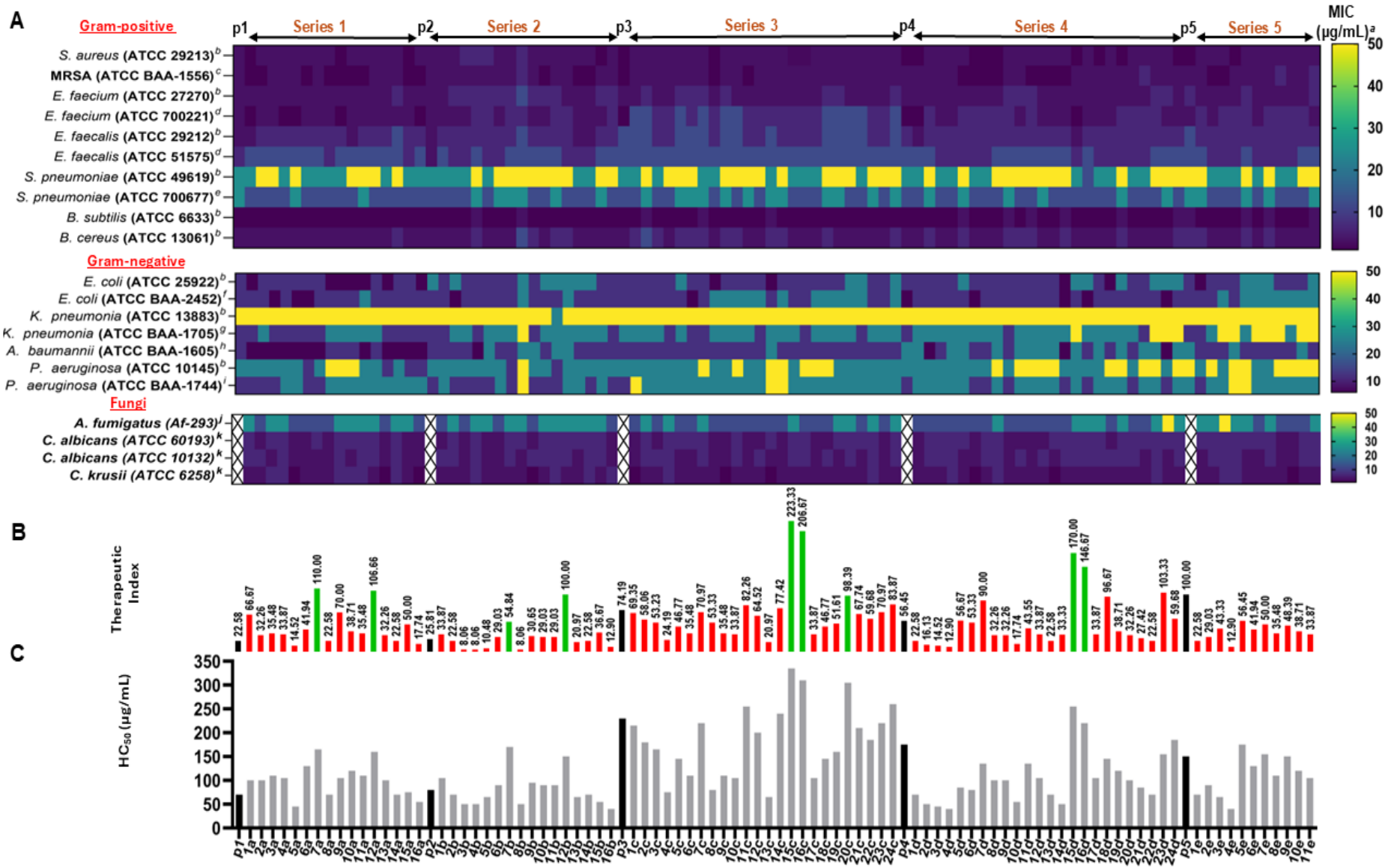

Figure 1. Antibacterial, antifungal, and hemolytic activity data of Series 1 (**1a-16a**), Series 2 (**1b-16b**), series 3 (**1c-24c**), Series 4 (**1d-24d**), and Series 5 (**1e-11e**), cyclic peptides and parent cyclic peptides (**p1**, **p2**, **p3**, **p4**, and **p5**) of each series. **(A)** [a]The minimum inhibitory concentration (MIC) heatmap of cyclic peptides against Gram-positive and Gram-negative bacterial strains and fungal strains. MIC is the lowest concentration of the peptides that inhibited bacterial growth. [b]Non-resistant (wild type) bacterial strain. [c]Methicillin-resistant *Staphylococcus aureus*. [d]Vancomycin-resistant *enterococci* strain. [e]Multi-drug resistant (Penicillin, Tetracycline, and Erythromycin) bacterial strain. [f]NDM-1, [g]Carbapenem, [h]Ciprofloxacin, [i]Imipenem resistant bacterial strains. [j]Multi-drug resistant clinical isolate of *A. fumigatus*. [k]Non-resistant (wild type) candida strains. The data represents the results of the experiments performed in triplicate.**(B)** The therapeutic index of each cyclic peptide is calculated by dividing HC_{50} with the MIC (observed against a representative Gram-positive strain *S. aureus* (ATCC 29213)) of each peptide. **(C)** Hemolytic activity of the peptides was determined using human red blood cells (hRBC) as HC_{50} values. The black color bar in each graph represents the HC_{50} and therapeutic index of parent peptides (**p1**, **p2**, **p3**, **p4**, and **p5**). Green color bars represent the peptides with high therapeutic index within the respective series. The data represents the experiment performed in triplicate.

2.2.2. Antifungal activity

The antifungal activity of the synthesized cyclic peptides (**1a-16a**, **1b-16b**, **1c-24c**, **1d-24d,** and **1e-11e**) was determined against *A. fumigatus* (Af-293) and two different strains of *C. albicans* (ATCC 60193, ATCC 10132) and one strain of *C. krusii* (ATCC 6258). The observed MICs are illustrated in Figure 1A and Table S5 in Supporting Information. Compared to *A. fumigatus*, *Candida* strains showed greater susceptibility against all the tested peptides. All peptides displayed good to moderate activity against *A. fumigatus* with MICs in the range of 12.5-50 µg/mL. Except for a few peptides that showed the highest activity against *C. Krusii* with MIC = 1.5 µg/mL, most of the tested peptides showed activity against *Candida* strains with MIC = 3.1-6.2 µg/mL.

2.3. Cytotoxicity

2.3.1. Hemolytic activity

The hemolytic activity of all the synthesized cyclic peptides was determined against the human red blood cells (hRBCs) as an *in vitro* cytotoxicity indicator. In Series 1, among the peptides designed by replacing one residue at a time with its D-isomer (**1a-7a**), peptide **7a**, having D-Arg at the first position, was found to be less hemolytic with HC_{50} = 165 µg/mL. A similar trend was observed for Series 2 peptides (**1b-7b**), with minimum hemolysis observed for **7b** (HC_{50} = 170 µg/mL). Noticeably, compared to their parent peptides **p1** and **p2**, **7a** and **7b**, respectively, displayed around twofold reduction in hemolytic activity (Figure 1C). Conversely, in Series 3 and 4, peptides designed by single enantiomeric replacements (**1c-7c** and **1d-7d**) did not show reduced toxicity compared to their respective controls, **p3** and **p4**. However, the peptides with D-Arg at the first position (**7c** and **7d**) exhibited the lowest hemolytic activity within their series (Figure 1C).

In Series 1 and 2, among the peptides containing multiple D-amino acid residues (**8a-16a** and **8b-16b**) demonstrated varying hemolytic activity. Compared to parent peptides **p1** and **p2**, the greatest reduction in hemolytic activity was observed for peptides **12a** (HC_{50} = 160 µg/mL) and **12b** (HC_{50} = 150 µg/mL), respectively (Figure 1C).

In Series 3, compared to parent peptide **p3** (HC_{50}=230 µg/mL), only a slight improvement in hemolytic activity was observed for peptides **11c** (HC_{50} = 255 µg/mL), **14c** (HC_{50} = 240 µg/mL), and **24c** (HC_{50} =260 µg/mL). However, significantly higher HC_{50} values were observed for **15c** (HC_{50} = 335 µg/mL), **16c** (HC_{50} = 310 µg/mL), and **20c** (HC_{50} = 305 µg/mL).

In Series 4, compared to parent peptide **p4** (HC_{50} = 175 µg/mL), most enantiomeric replacements resulted in increased hemolytic activity. However, slight reductions in hemolytic potential were observed for **15d** (HC_{50} = 255 µg/mL) and **16d** (HC_{50}=220 µg/mL). In Series 5, compared to parent peptide **p5** (HC_{50} = 150 µg/mL), its enantiomeric analogs displayed either closely similar (**5e**, **7e**, and **9e**) or higher (**1e**-**4e**, **6e**, **8e**, **10e**, and **11e**) hemolytic activity.

For further studies, peptides were selected based on the therapeutic index. For each cyclic peptide, the therapeutic index was calculated by dividing HC_{50} values by the MICs against *S. aureus* (ATCC 29213). The therapeutic index values are presented as a bar graph, with peptides showing higher therapeutic index in each series (**7a**, **12a**, **7b**, **12b**, **15c**, **16c**, **20c**, **15d**, and **16d**) highlighted in green (Figure 1B). Peptides with higher therapeutic index were selected for broad-spectrum antimicrobial activity and cell cytotoxicity studies.

The therapeutic index of each cyclic peptide was determined by dividing the HC_{50} value by the MIC, measured against the representative Gram-positive strain *S. aureus* (ATCC 29213) (Figure 1B), where HC_{50} represented the hemolytic activity of the peptides using human red blood cells (hRBC) (Figure 1C). Cyclic peptides with a higher therapeutic index (**7a**, **12a**, **7b**, **15c**, **16c**, and **20c**) were selected for further antibacterial screening against a broader range of Gram-positive and Gram-negative bacteria.

2.3.2. Cell viability assay

Based on the hemolysis data, we selected peptides that displayed a significant reduction in hemolytic activity compared to their respective control peptides for extensive cytotoxicity evaluation against four different normal mammalian cells.

In Series 1 and 2, similar to hemolysis data, **7a**, **12a**, **7b**, and **12b** showed a significant improvement in cytotoxicity against all four types of normal mammalian cells compared to the parent peptides (**p1** and **p2)** (Figures 2A1-A4, B1-B4). For instance, at 150 µg/mL, 30-35% cell viability was observed for control peptides **p1** and **p2** against lung cells, whereas peptides **7a**, **12a**, **7b**, and **12b** showed twofold improvement, with 61-70% cell viability.

In Series 3 and 4, all the tested cyclic peptides showed higher cell viability against all four mammalian cells compared to their respective parent peptides (Figures 2C1-C4, D1-D4). In Series 3, among the tested cyclic peptides (**15c**, **16c**, and **20c**), consistently higher cell viability was observed for **15c** and **16c** against all four types of mammalian cells compared to **20c**. At 200 µg/mL, cyclic peptides **15c** and **16c** displayed 76-81%, 72-77 %, 80-82%, and 64-69% cell viability against lung, kidney, liver, and skin cells, respectively. However, compared to parent peptide **p3**, at 200 µg/mL **20c** showed only a marginal improvement, if any, with

62%, 55%, 73%, and 49% cell viability against lung, kidney, liver, and skin cells, respectively. Moreover, it is important to note that except for skin cells, at 100 µg/mL, **15c** and **16c** showed >90% cell viability against lung, kidney, and liver cells (Figures 2C1-C4).

Similarly, in Series 4, peptides **15d** and **16d** showed higher cell viability compared to the parent peptide **p4** with 61-65%, 67-72%, 74-77%, and 47-50% cell viability at 200 µg/mL against lung, kidney, liver, and skin cells respectively (Figures 2D1-D4). Among all the tested cyclic peptides, maximum cell viability was observed for **15c** and **16c**, aligning well with the hemolysis data.

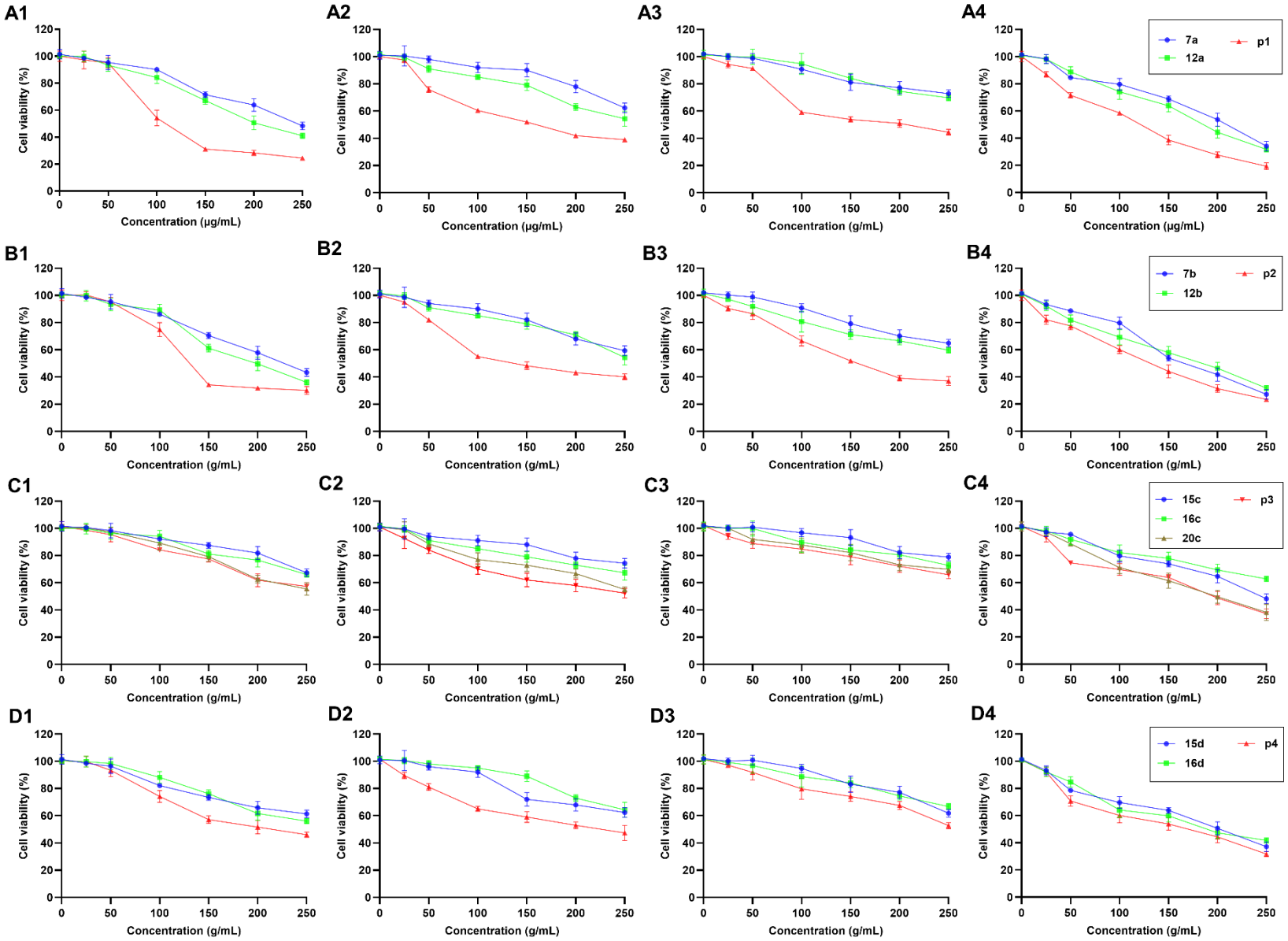

Figure 2. Percentage cell viability data of selected cyclic peptides from Series 1 (**7a** and **12a**), Series 2 (**7b** and **12b**), Series 3 (**15c**, **16c**, and **20c**), and Series 4 (**15d** and **16d**) and their respective parent peptide (**p1, p2, p3,** and **p4)** incubated for 24 h against human lung cells (MRC-5) (A1, B1, C1, and D1), Embryonic kidney (HEK-293) (A2, B2, C2, and D2), liver cells (HPRGC10) (A3, B3, C3, and D3), and Skin fibroblast cells (HeKa) (A4, B4, C4, and D4). The results represent the data obtained from the experiments performed in triplicate.

2.4. Antibacterial and antifungal activity of selected peptides against a broader range of pathogens

Peptides with higher therapeutic indexes (**7a**, **12a**, **7b**, **15c**, **16c**, and **20c**) were selected for broad-spectrum antimicrobial activity. The extended-spectrum screening experiments were conducted by JMI Laboratories (North Liberty, IA) and subcontracted by the National Institute of Health. The activity results are illustrated in Table 1. Except **16c**, all selected peptides showed good activity against methicillin-susceptible (MSSA) (ATCC 29213), methicillin-resistant (MRSA) (1193193), and multi-drug resistant (MDR) *S. aureus* (1195201) with MICs of 4 µg/mL. Noticeably, while all peptides displayed a comparable activity to classical antibiotic meropenem, they demonstrated 4- to 8-fold higher activity against MRSA and MDR *S. aureus* compared to cefepime (Table 1). Except for **7b** against *A. baumannii* (1188767), all selected cyclic peptides showed moderate activity (MIC = 8-32 µg/mL) against all the tested strains of *E. coli* and *A. baumannii*. Consistent with the activity data mentioned above (Figure 1A), the peptides showed lower potency against all tested strains of *P. aeruginosa* and *K. pneumoniae* compared to *E. coli* and *A. baumannii*. Overall, these activity results closely align with the activity data obtained in our in-house conducted activity.

Table 1. Antibacterial activity of selected cyclic peptides.

Bacterial Strain	MIC (μg/mL)[a]										
	7a	**12a**	**7b**	**15c**	**16c**	**20c**	**Cefepime**	**Colistin**	**Levofloxacin**	**Meropenem**	**Oxacillin**
S. aureus[b] (ATCC 29213)	4	4	4	4	4	4	2	ND	0.12	0.06	0.25
S. aureus[c] (1193193)	4	4	4	4	8	4	16	ND	0.25	2	>4
S. aureus[d] (1195201)	4	4	4	4	8	4	>32	ND	0.25	4	>4
E. coli[b] (ATCC 25922)	16	32	16	16	16	16	0.06	0.25	≤0.03	0.15	ND
E. coli[c] (ATCC BAA-2452)	8	16	16	16	8	8	32	≤0.12	≤0.03	>8	ND
E. coli[d] (1191008)	16	32	32	16	8	16	8	0.25	>8	0.015	ND
A. baumannii[e] (NCTC 13304)	16	16	16	16	8	16	32	0.5	8	>8	ND
A. baumannii[d] (1188767)	16	8	>64	8	8	32	32	0.25	4	>8	ND
A. baumannii[d] (1189854)	8	8	16	8	8	8	32	4	>8	>8	ND
P. aeruginosa[b] (ATCC 27853)	32	16	32	32	64	64	1	0.5	1	0.25	ND
P. aeruginosa[d] (1188712)	32	32	16	32	32	32	8	1	>8	8	ND
P. aeruginosa[d] (1191191)	8	8	32	32	>64	32	32	0.5	2	>8	ND
K. pneumonia[f] (ATCC BAA1705)	>64	>64	64	32	>64	>64	32	≤0.12	>8	>8	ND
K. pneumonia[g] (ATCC 700603)	64	64	64	16	32	>64	1	0.25	0.5	0.03	ND
K. pneumonia[d] (1188718)	>64	>64	>64	>64	>64	>64	8	≤0.12	1	0.03	ND

[a]The minimum inhibitory concentration (MIC) is the lowest concentration of the peptides that inhibited bacterial growth. [b]Non resistant (wild type) bacterial strain. [c]Methicillin-resistant *Staphylococcus aureus*. [d]Multi-drug-resistant *Staphylococcus aureus*. [c]Carbapenem, New Delhi metallo-beta-lactamase (NDM-1)-positive resistant bacterial strain (CRE (NDM-1)). [d]Multi-drug resistant bacterial strain. [e]Carbapenem resistant bacterial strain. [f]Carbapenem-resistant Enterobacterales (KPC-2). [g]Extended-spectrum β-lactamase (ESBL) (*K. pneumoniae* ATCC 700603 produces SHV-18). [i]Results of the assays conducted by NIH. [j]ND, not determined. The data represents the results of two independent experiments performed in triplicate.

Among all the cyclic peptides, those with a higher therapeutic index (**7a**, **12a**, **7b**, **15c**, **16c**, and **20c**) were selected for further evaluation against a wider range of fungi. The assays were performed by JMI Laboratories (North Liberty, IA) and subcontracted by the National Institute of Health (Table 2). Among all the tested fungal strains, the highest activity was observed against the three tested strains of *Blastomyces dermatitidis* with MICs = 0.5-4 µg/mL. In addition, all the tested peptides displayed good activity against *Paecilomyces variotii* and *Candida parapsilosis* with MIC = 4-16 µg/mL. While no activity was observed against the tested strains of *A. fumigatus* (DI15-116) (MIC ≥ 64 µg/mL), good to moderate activity was observed against the *Candida* strains (MIC = 8-32 µg/mL). Noticeably, against *Paecilomyces variotii*, while **7a** showed one-fold higher activity (MIC = 4 µg/mL), the rest of the tested peptides displayed the same activity as that of standard antibiotic fluconazole with MIC =8 µg/mL (Table 2).

Table 2. Antifungal activity of selected cyclic peptides.[a]

Species	**MIC (µg/mL)[b]**							
	7a	**12a**	**7b**	**15c**	**16c**	**20c**	Fluconazole	Voriconazole
Candida albicans (SC5314)	16	32	16	16	16	32	0.5	ND[c]
Candida albicans (CA90028)	8	8	8	8	16	16	0.25	ND[c]
Candida albicans (CA3)	16	32	16	32	32	32	>64	ND[c]
Candida parapsilosis (ATCC 22019)	4	8	8	16	16	16	1	ND[c]
Paecilomyces variotii (MYA-3630)	4	8	8	8	8	8	8	0.06
Blastomyces dermatitidis (BD-1)	0.5	1	2	2	1	2	ND[c]	0.06
Blastomyces dermatitidis (BD-2)	1	1	2	1	1	2	ND[c]	≤0.03
Blastomyces dermatitidis (BD-3)	2	2	4	4	2	2	ND[c]	≤0.03
Aspergillus fumigatus (DI15-106)	64	>64	>64	>64	>64	>64	ND[c]	>16
Aspergillus fumigatus (DI15-116)	>64	>64	>64	>64	>64	>64	ND[c]	4

[a]Results represent the highest MIC value obtained from three independent experiments performed in triplicate. [b]Minimum inhibitory concentrations (MIC) were determined as the lowest concentration of the peptides that inhibited fungal growth. [c]ND represents not determined.

2.5. Kill-kinetic assay

Among all the selected compounds, **15c** and **16c** were advanced for further biological studies. The kinetics of bactericidal and fungicidal action of **15c** and **16c** were determined against MRSA (ATCC BAA-1556) (Figure 3A1), *E. coli* (ATCC BAA-2452) (Figure 3A2), *A. fumigatus* (Af 293) (Figure 3A3), and *C. albicans* (ATCC 60193) (Figure 3A4). The results of the kill kinetic assay revealed the rapid killing action of **15c** and **16c** against both bacteria and fungi, which was either comparable or even better than the standard antibiotics (Figures 3A1-A4).

At MIC, both **15c** and **16c** exerted the complete eradication of MRSA (Figure 3A1) and *E. coli* (Figure 3A2) in 3-4 h. On the other hand, at 4×MIC both **15c** and **16c** induced complete neutralization of bacterial burden (MRSA and *E. coli*) after 2 h of treatment. Moreover, it is important to note that at 4×MIC, both **15c** and **16c** induced eradication of >85% of MRSA cells after 1 h treatment (Figure 3A1). However, at MIC and 4×MIC, standard antibiotics daptomycin and polymyxin B exerted complete killing of MRSA (Figure 3A1) or *E. coli* (Figure 3A2) in 4-5 h and 3 h, respectively.

Compared to their bactericidal effects, moderate fungicidal action was observed for **15c** and **16c** against both *A. fumigatus* (Figure 3A3) and *C. albicans* (Figure 3A4). Exposure of *A. fumigatus* and *C. albicans* to **15c** and **16c** at MIC for 12 h resulted in >65% reduction in the number of viable fungal cells. However, treatment with standard antibiotics amphotericin B and fluconazole at MIC for 12 h induced a 40-45% reduction in viable *A. fumigatus* (Figure 2A3) and *C. albicans* (Figure 3A4), respectively.

At 4×MIC, **15c** and **16c** neutralized >85% of fungal cells after 8 h and exerted complete or >95% eradication after 12 h of treatment. The full eradication was observed as early as 10 h. On the other hand, treatment of *A. fumigatus* and *C. albicans* with amphotericin B and fluconazole, respectively, at 4×MIC for 12 h resulted in around 65-70% reduction of viable cells (Figures 3A3 and A4). The kill-kinetic assay data revealed the superior bactericidal and fungicidal action of cyclic peptides **15c** and **16c** compared to the respective standard antibiotics used in the study.

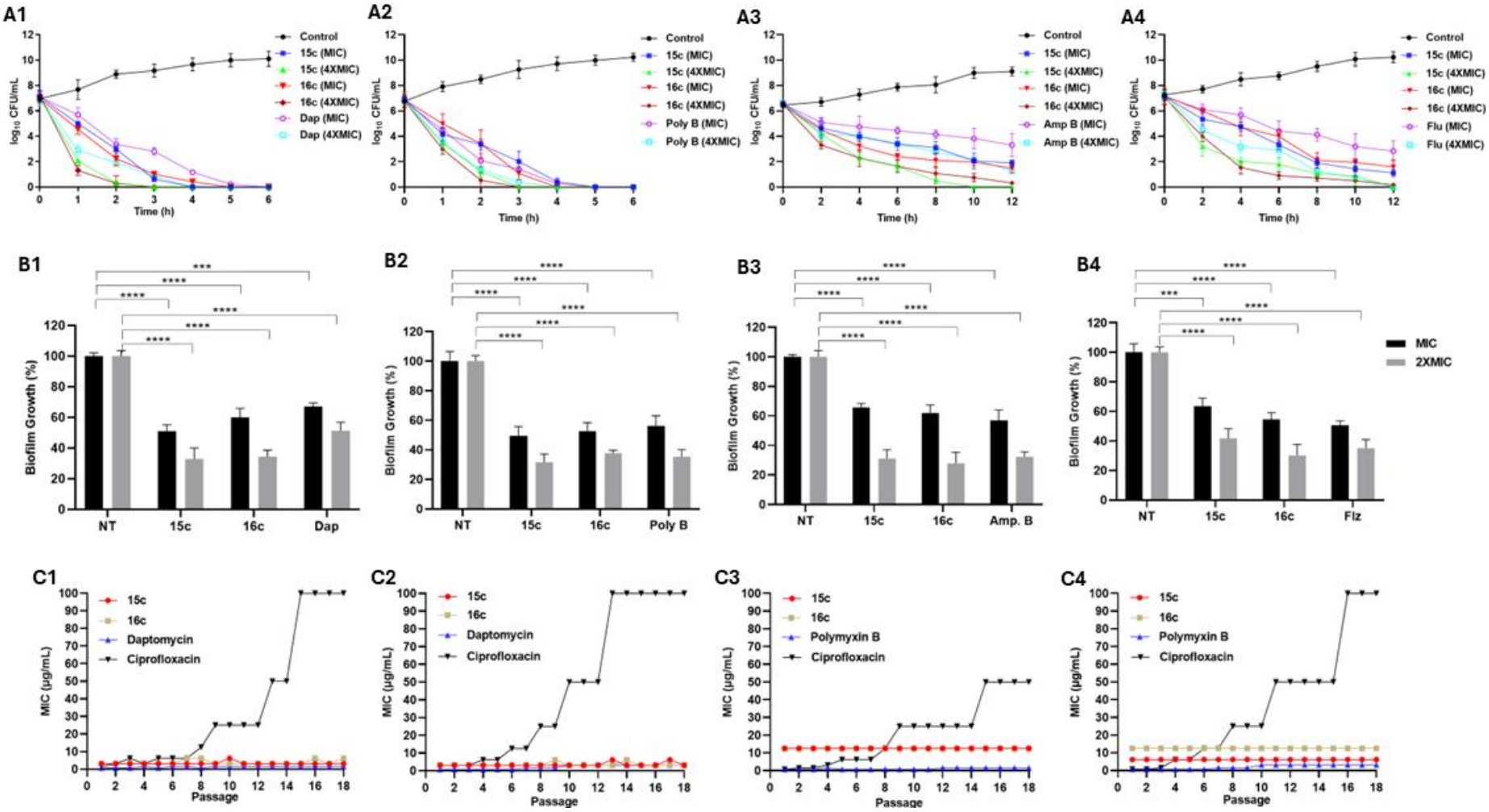

Figure 3. (A) Time-dependent killing action of the lead macrocyclic peptides (**15c** and **16c**) and standard antibiotics, daptomycin and polymyxin B, against bacteria (A1 (MRSA (ATCC BAA-1556)) and A2 (*E. coli* (ATCC BAA-2452)) and fungi (A3 (*A. fumigatus* (Af-293)) and A4 (*C. albicans*) (ATCC 60193)) at MIC and 4×MIC. The data obtained are from the experiments performed in triplicate. **(B)** Antibiofilm activity of lead peptides (**15c** and **16c**) against bacteria (B1 (MRSA (ATCC BAA-1556)), B2 (*E. coli* (ATCC BAA-2452)) and fungi (B3 (*A. fumigatus* (Af 293), B4 (*C. albicans* (ATCC 60193)) at MIC and 2×MIC. NT corresponds to the negative control-untreated cells in PBS. Standard antibiotics daptomycin (Dap), polymyxin B (Poly B), amphotericin B (Amp B), and fluconazole (Flz) were used as a positive control against bacteria and fungi, respectively. The data obtained are from the experiments performed in triplicate. The data were analyzed using a two-tailed unpaired Student's *t*-test (***$p < 0.001$ and ****$p < 0.0001$). **(C)** Resistance induction after repeated 18 times exposures of lead cyclic peptide (**15c** and **16c)** and standard antibiotics (daptomycin, polymyxin B, and ciprofloxacin) against *S. aureus* (ATCC 29213) (C1), MRSA (ATCC BAA-1556) (C2), *E. coli* (ATCC 25922) (C3), and *E. coli* (ATCC BAA-2452) (C4). The data represents the experiments conducted in triplicate.

2.6. Anti biofilm activity

The anti-biofilm potential of lead cyclic peptides (**15c** and **16c**) was determined against bacterial strains MRSA (ATCC BAA-1556) (Figure 3B1) and *E. coli* (ATCC BAA-2452) (Figure 3B2), as well as fungal strains *A. fumigatus* (Af 293) (Figure 3B3) and *C. albicans* (ATCC 60193) (Figure 3B4), at MIC and 2×MIC. The ability of test compounds (lead cyclic peptides and standard antibiotics) to inhibit biofilm was determined by conducting an XTT assay, and the results were represented as the percent reduction in the biofilm mass relative to non-treated cells.

At MIC, lead cyclic peptides **15c** and **16c** showed good anti-biofilm activity against MRSA (Figure 3B1) and *E. coli* (Figure 3B2) with around 41-49% decrease in biofilm mass compared to non-treated cells. For both **15c** and **16c**, at 2× the MIC, a higher anti-biofilm activity was observed with a 63-69% decrease in biofilm mass. Noticeably, compared to **15c** and **16c**, slightly less antibiofilm activity was observed for daptomycin, with around 33% and 49% decrease in biofilm mass of MRSA at MIC and 2× the MIC, respectively (Figure 3B1). In contrast, polymyxin B displayed marginally higher anti-biofilm activity than daptomycin against *E. coli*, with reductions of 44% at MIC and 65% at 2× MIC. These values were comparable to those observed for lead cyclic peptides **15c** and **16c** (Figure 3B2).

A similar trend in anti-biofilm activity was observed for both **15c** and **16c** against fungi, with a significant decrease in the biofilm mass of both *A. fumigatus* (Figure 3B3) and *C. albicans* (Figure 3B4). In comparison to untreated cells, *A. fumigatus* treated with **15c** and **16c** at MIC resulted in 35-38% reduction in biofilm mass. Notably, at 2× the MIC, **15c** and **16c** induced approximately two-fold greater reduction in biofilm mass (69-73%) of *A. fumigatus.*

For *C. albicans*, peptide **16c** demonstrated slightly higher anti-biofilm activity than **15c**. Compared to the non-treated cells, while **15c** at MIC and 2× the MIC induced 37% and 59% decrease in biofilm mass, **16c** exerted 46% and 70% decrease in biofilm mass, respectively. In contrast, standard antibiotics, amphotericin B and fluconazole, showed closely similar anti-biofilm activity against *A. fumigatus* and *C. albicans* with 44-50% and 65-68% decrease in biofilm mass at MIC and 2× the MIC, respectively (Figures 3B3 and 3B4). Overall, **15c** and **16c** displayed remarkable anti-biofilm activity against both bacterial and fungal strains, which were comparable to standard antibiotics.

2.7. *Evaluation of the pathogen's ability to develop resistance*

Repeated use of antibiotics usually leads to resistance development. By repeated exposure with lead cyclic peptides (**15c** and **16c**), we examined the resistance development potential of resistant and susceptible strains of both Gram-positive bacteria, *S. aureus* (ATCC 29213) (Figure 3C1) and MRSA (ATCC BAA-1556) (Figure 3C2), and Gram-negative bacteria, *E. coli* (ATCC 25922) (Figure 3C3) and *E. coli* (ATCC 25922) (Figure 3C4). Standard antibiotics, daptomycin, polymyxin B, and ciprofloxacin, were included as positive controls.

After each round of bacterial exposure to test peptides or standard antibiotics, the new MIC was determined as an indicator of resistance development. Interestingly, similar to the peptide-based antibiotics (daptomycin and polymyxin B), negligible changes in the MICs were observed for peptides **15c** and **16c** against all the tested bacterial strains. However, a continuous increase in the MICs of ciprofloxacin was observed against all the tested bacterial strains (Figures 3C1-3C4). Overall, these results indicated that both Gram-positive and Gram-negative pathogens are unable to develop resistance against **15c** and **16c**.

2.8. Membranolytic action of the lead peptides

2.8.1. Calcein dye leakage assay

The membranolytic action of lead cyclic peptides **15c** and **16c** was accessed by conducting a calcein dye leakage assay using lipid vesicles mimicking bacterial and mammalian membranes. The fluorescent dye leakage experiments showed that both **15c** and **16c** induced a concentration-dependent dye leakage when treated with bacterial membrane-mimicking liposomes. At 50 µg/mL, cyclic peptides **15c** and **16c** resulted in the leakage of 56-64% of dye after 20 min exposure to bacterial mimicking liposomes and induced 100% dye release after 60 min and 50 min, respectively. At the lowest experimental concentration (5 µg/mL), both cyclic peptides (**15c** and **16c**) exerted the disruption of lipid vesicles as indicated by 38% of dye release after 50 min incubation (Figures 4A1 and A2).

Compared to cyclic peptides **15c** and **16c**, a rather mild dye leakage action was observed for daptomycin, with only 34% of dye release at 50 µg/mL after 100 min incubation with bacterial membrane mimicking liposomes (Figure 4A3). Noticeably, when treated with mammalian membrane mimicking liposomes, both **15c** and **16c**, even at the highest experimental concentration (50 µg/mL), induced insignificant dye leakage as evidenced by 12-18% dye release after 100 min exposure (Figures 4A4 and A5). Similarly, a negligible amount of dye leakage (around 6% at 50 µg/mL after 100 min) was observed for daptomycin when incubated with mammalian mimicking liposomes (Figure 4A6).

The results of calcein dye leakage experiments indicated that **15c** and **16c** possess a predominant preference towards bacterial over mammalian membrane cells, and like most of the native AMPs, the antibacterial activity was dependent on their ability to permeate through the target membranes.

2.8.2. Field-Emission Scanning Electron Microscopy (FE-SEM)

To study the membrane-damaging action of lead cyclic peptides (**15c** and **16c**) on live microbial cells, we used SEM to examine untreated and treated bacterial and fungal cells. The untreated microbial cells displayed smooth, intact surfaces and regular morphology (Figures 4B1, B4, B7, and B10). In contrast, treated microbial cells, especially bacteria, were visualized to have significant structural damage.

For treated MRSA cells, membrane disruption was clearly evident with intracellular contents visibly oozing out (Figures 4B2 and B3). Treated *E. coli* cells displayed even more pronounced morphological changes, including cell shrinkage and the formation of surface blisters (Figures 4B5 and B6). Surface irregularities, such as blebs and wrinkles, were spotted on the surface of treated *A. fumigatus* cells (Figures 4B8 and B9), while similar morphological deformities were observed for the treated *C. albicans* (Figures 4B11 and B12).

Overall, these morphological changes and structural damages were consistently observed among all treated microbial cells. Together with the results from the calcein dye leakage assay data, the SEM micrographs provide further confirmation of the membranolytic activity of **15c** and **16c**.

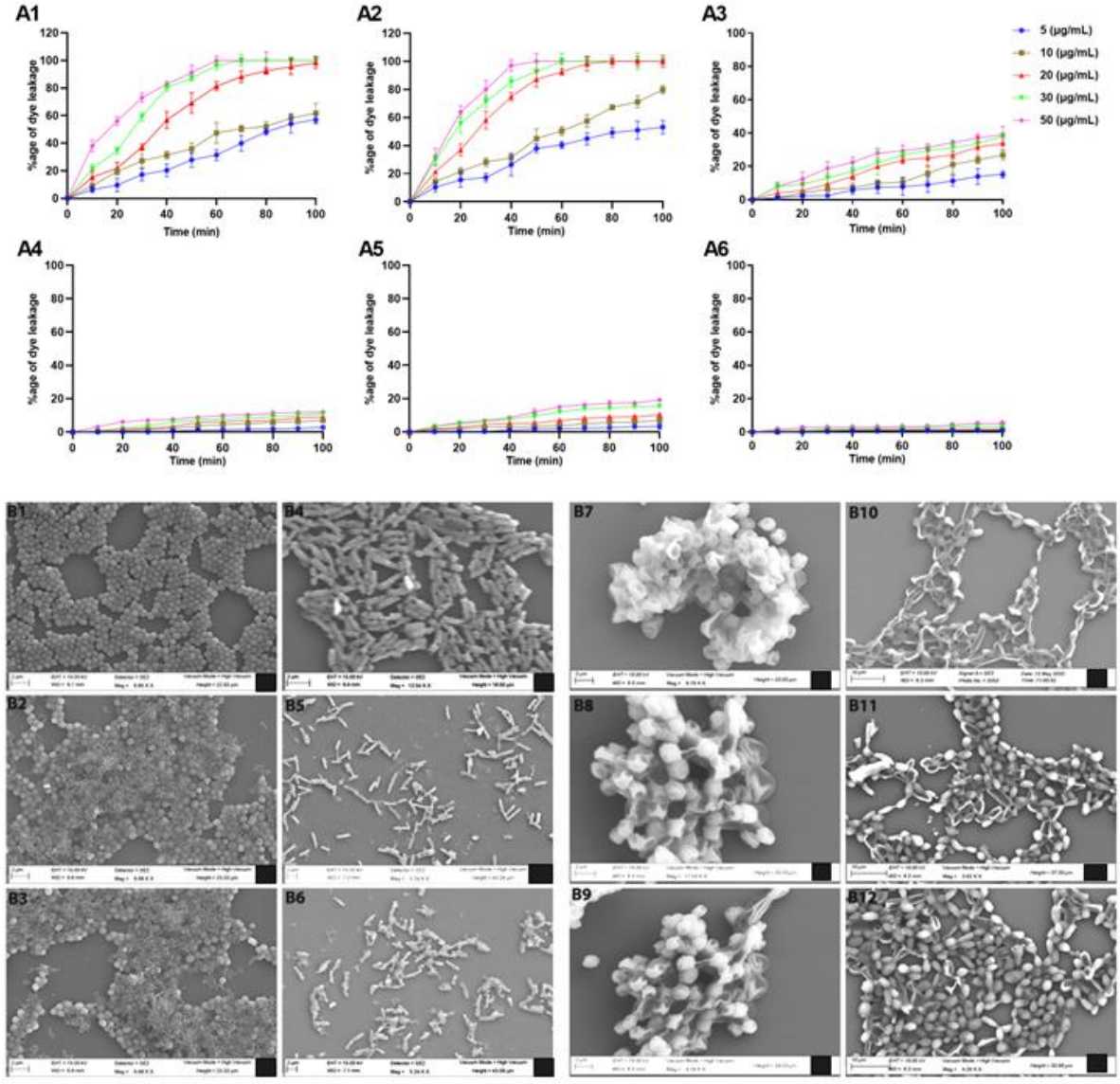

Figure 4. **(A)** Concentration-dependent leakage of calcein dye from bacterial membrane mimicking (A1-A3) and mammalian membrane mimicking (A4-A6) liposomes. **15c** (A1 and A4); **16c** (A2 and A5); daptomycin (A3 and A6). The data obtained are from the experiments performed in triplicate. **(B)** FE-SEM images of bacteria (MRSA (B1-B3) and *E. coli* (B4-B6)) and fungal (*A. fumigatus* (B7-B9) and *C. albicans* (B10-B12)) cells treated with lead macrocyclic peptide **15c** (B2, B5, B8, and B11) and **16c** (B3, B6, B9, and B12) at 4×MIC for 1 h. The control for each bacterial (B1 and B4) and fungal (B7 and B10) strain was done without peptide.

2.9. Plasma stability study

The enzymatic stability of lead cyclic peptides (**15c** and **16c**) against peptidases was determined by incubating them in human plasma and analyzing them at different time intervals for 24 h. The percentage of peptides that remained undegraded at different time points was

determined by measuring the area under the curve in the extracted ion chromatogram (EIC, Figure 5).

After 30 min incubation, approximately 83.1% and 90.4% of undegraded **15c** and **16c** were observed, respectively. Compared to **16c**, a slightly higher enzymatic susceptibility was observed for **15c**, as indicated by 50.7% and 59.1% of **15c** and **16c**, respectively, remaining undegraded after 6 h incubation. After 24 h incubation, 31.2% and 37.7% of **15c** and **16c**, respectively, remain undegraded. The data suggested that **15c** and **16c** demonstrate good stability in human plasma with a half-life ($t_{1/2}$) of 6 h and 8 h, respectively.

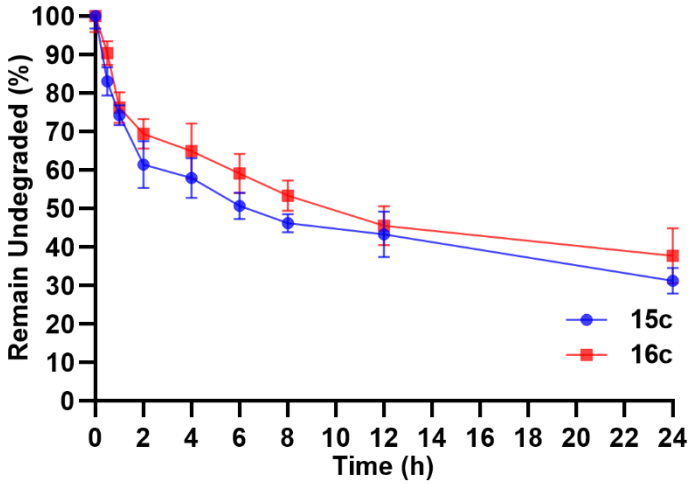

Figure 5. *In vitro* plasma stability assay of the lead cyclic peptide **15c** and **16c**. The data represents the percentage of undegraded peptides measured using Q-TOF LC/MS as the area under the curve in the extracted ion chromatogram in three independent experiments.

2.10. Analysis of structure and oligomerization by NMR spectroscopy

Peptides **15c** and **16c** were identified as the leading peptides based on their antimicrobial activity and low cytotoxicity. NMR analysis revealed that their interactions with liposomes mimicking bacterial or mammalian membranes were consistent with the previously described behavior of other short amphiphilic cyclic peptides.[30, 32] Specifically, both peptides interacted effectively with the bacteria-mimicking liposomes while demonstrating minimal binding to the mammalian-mimicking liposomes (Supplementary Figure S4).

To further investigate the impact of amino acid and L/D-isomeric replacements on the peptide properties, we systematically compared the behavior and structural features of the lead

peptide **15c** and its prototypes, **p1**[30] and **p3**[32], in water and in the presence of membrane mimetics by NMR spectroscopy.

First, to assess the differences in the peptides' structures and aggregation in water, we assessed the solvent accessibility for H^N atoms of the backbone and the effects of the size of the peptide oligomers or aggregates on the ^{1}H-NMR line shapes. We utilized a combination of 1D and 2D ^{1}H-NMR experiments.

The first indication of the distinct structural behavior of the peptides was observed in ^{1}H-NMR experiments. The line widths of most of the HN signals in the samples of the peptides **p3** and **15c** at all used concentrations were much lower (8-10 Hz for **p3** and below 8 Hz for **15c**) than for peptide **p1** (15-20 Hz, Figure 6). For the peptides of this size (MW of about 1300 Da), line widths of the backbone H^N signal exceeding 20 Hz indicate the presence of high-order oligomers or aggregates.

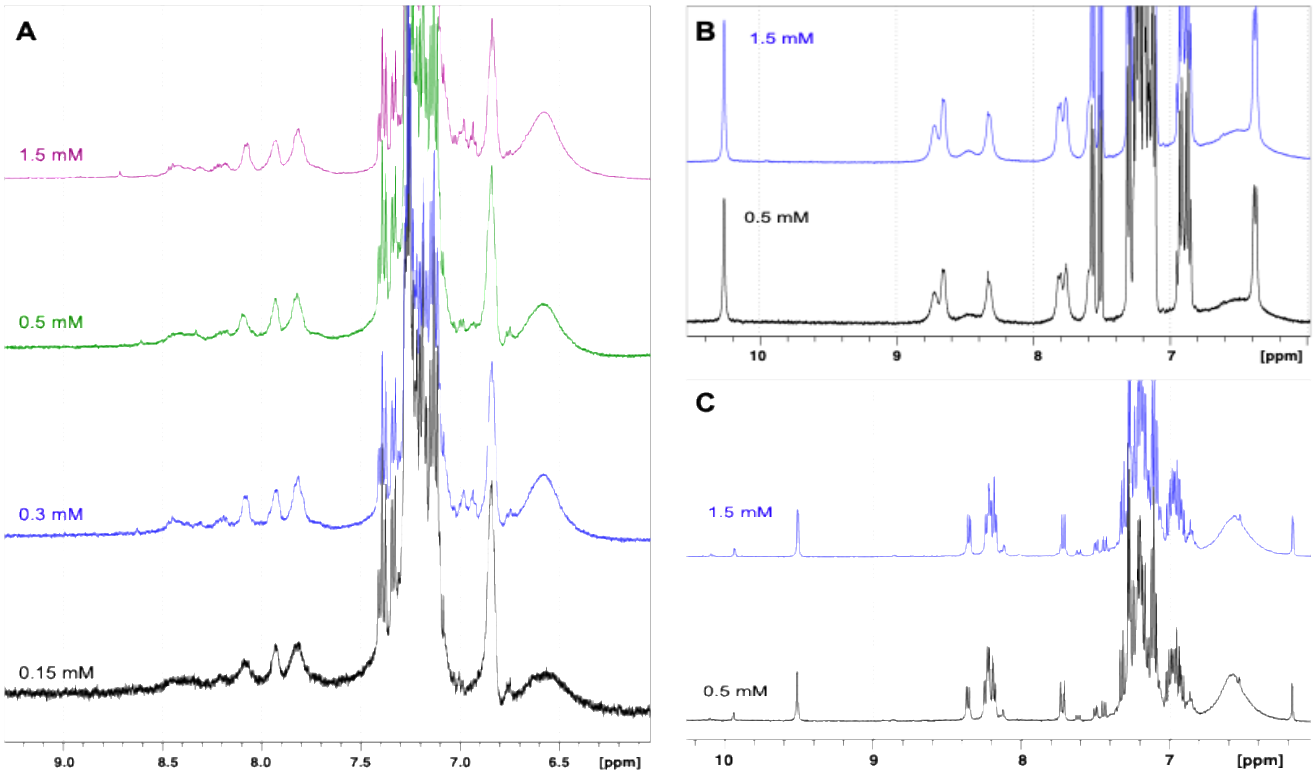

Figure 6 ^{1}H-NMR spectra of peptides **p1** (A), **p3** (B), and **15c** (C) at different concentrations in water. Concentrations are shown with the spectrum colors. The spectra are scaled to match signal intensity at different concentrations.

Further analysis of the exchange cross-peaks between backbone H^N protons and water in 2D spectra showed that in peptide **p1** at concentrations above 0.3 mM, only the sidechain $H^{N\varepsilon}$ of all Arg residues were solvent-accessible. All backbone H^N groups were shielded and showed no interaction with water, potentially due to oligomerization or aggregation (Figure 7A).

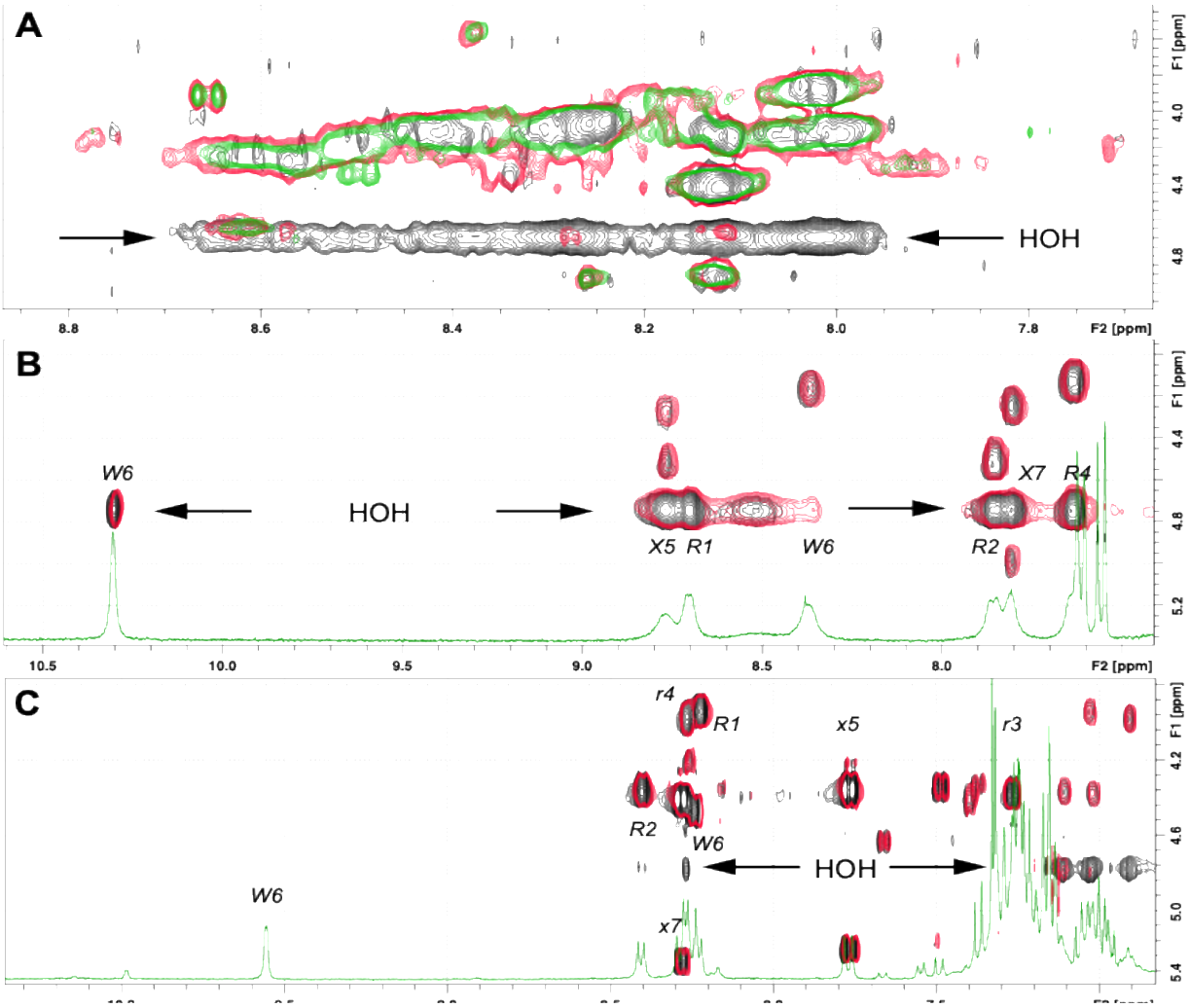

Figure 7. 2D ^{1}H-NMR TOCSY spectra of peptides **p1 (A)**, **p3 (B)**, and **15c (C)** in water. Peptide concentrations are: **p1** - 1.5 mM (green), 0.5 mM (red), 0.15 mM (black); **p3** and **15c** - 1.5 mM (red) and 0.5 mM (black). 1D ^{1}H-NMR spectra (green) and positions for H^N resonances are shown for peptides **p3** and **15c** with residue labels for reference. Low case letters correspond to D-amino acids, "*X*" and "*x*" correspond to Dip residues. The position of the water signal is shown with black arrows. The spectra are scaled to match signal intensity at different concentrations.

At a concentration of 0.15 mM, unlike higher concentrations, all backbone H^N groups in peptide **p1** exhibited exchange cross-peaks with the water signal in the TOCSY and NOESY spectra, confirming their solvent exposure (Figure 7A). Thus, we can estimate that strong

oligomerization of peptide **p1** in water occurs at a concentration of 0.15-0.30 mM. Furthermore, a detailed analysis of 2D NOESY spectra of peptide **p1** did not reveal any cross-peaks between H^N atoms of the peptide, suggesting no preferable stable conformation of the backbone in the aggregated and low-oligomeric states.

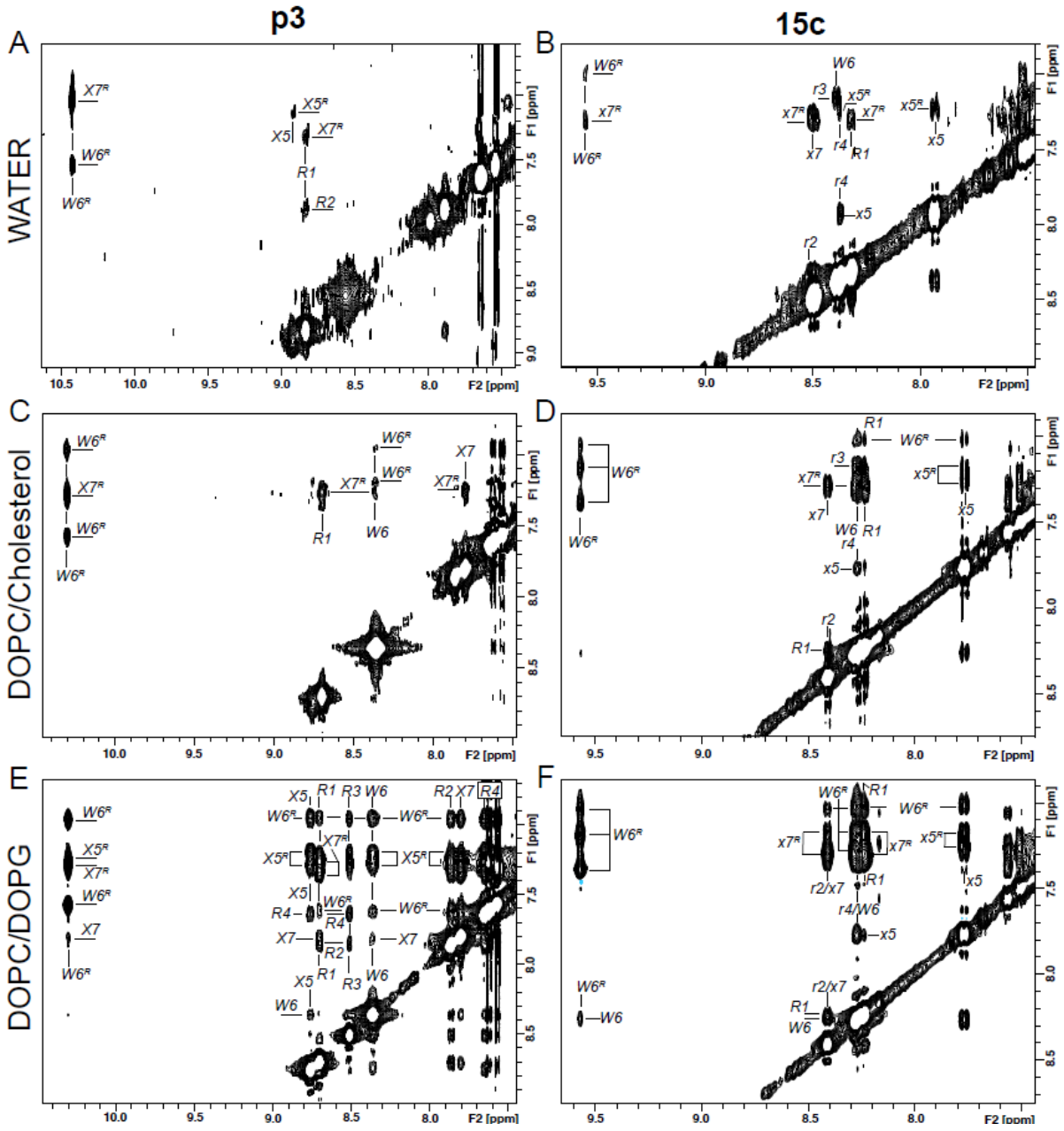

Figure 8. 2D ^{1}H-NMR NOESY spectra of peptides **p3** (Left column, panels A, C, E) and **15c** (Right column, panels B, D, F) in water (top row, A-B) and in the presence of mammalian membrane mimics (DOPC/cholesterol, middle row, C-D) and bacterial membrane mimics (DOPC/DOPG, bottom row, E-F). NOESY spectra in water were collected at 278K, and the spectra in the presence of liposomes were collected at 298K. The cross-peaks are marked with residue labels for H^N and with additional "*R*" for aromatic ring resonances. Low case letters indicate *D*-amino acids, "*X*" and "*x*" correspond to Dip residues.

In contrast to peptide **p1**, even at the highest used concentration of 1.5 mM, H^N groups of residues Arg1, Arg2, Arg4, Dip5, and Dip7 in peptide **p3** demonstrate strong exchange cross-peaks with water in TOCSY spectra (Figure 7B). These cross-peaks, as well as the H^N signal linewidths (around 8-10 Hz), indicate that **p3** exists in a low-oligomeric state, with its backbone partially exposed to solvent. Peptide **15c** demonstrates behavior similar to **p3** at all tested concentrations, with linewidths below 8 Hz, which corresponds to the monomeric (or very low oligomeric) form of the peptide. Additionally, exchange cross-peaks with water were detected for the backbone H^N groups of Arg2 and Arg4 at both tested concentrations (Figure 7C).

Upon interaction with the lipids mimicking bacterial membrane, peptides **p3** and **15c** produce an enhanced network of NOE contacts between H^N atoms as well as multiple interactions between H^N atoms and aromatic side chains. The NOESY spectrum for **p3** in the presence of DOPC/DOPG mixture showed continuous contacts for all neighboring H^N-H^N as well as contacts between all H^N atoms and the three aromatic side chains (Figure 8E).

Although signal overlap complicated the analysis of the NOESY spectra for peptide **15c**, we identified H^N-H^N cross-peaks (or overlapping potential cross-peaks) between all neighboring H^N atoms and between all H^N atoms and aromatic side chains (Figure 8F). In contrast, for **p3** in water, only H^N-H^N contact between Arg1 and Arg2 and contacts between H^N of Arg1 and Dip7 side chain, as well as between H^N and the side chain of Dip5, were detected (Figure 8A). For **p3** in the presence of DOPC/cholesterol liposomes mimicking mammalian membrane (Figure 8C), only a few contacts between backbone HNs and aromatic side chains were found, including Arg1-Dip7 and intra-residue contacts between Trp6 and Dip7. For **15c**, a similar network of contacts was detected in water and in the presence of DOPC/cholesterol liposomes. These included sequential H^N-H^N contacts between Arg1-arg2, arg4-dip5, and dip5-Trp6; contacts between H^N atoms and aromatic side chains of dip5, Trp6, and dip7 as well as between Arg1 and the side chain of dip7 (Figures 8B and D).

In summary, peptide **15c** exhibits a minimal tendency to aggregate in water and has a more structurally stable backbone than **p1**. Even in monomeric or low oligomeric states, substantial parts of the backbones in **p3** and **15c** are protected from solvent due to more stable conformations and more efficient shielding by the aromatic side chains, unlike **p1**. In water, peptide **15c** shows a more structured backbone, particularly in the stable regions Arg1-Arg2 and arg4-Dip5, whereas **p3** has only one short stable region Arg1-Arg2. Peptide **p1** has the

highest tendency for aggregation (at concentrations of 0.3 mM and above), with all backbone amides shielded from the solvent in the aggregated state. However, in the non-aggregated state (at 0.15 mM), the full exposure of all backbone amides to water indicates high backbone flexibility and less effective hydrophobic shielding by its side chains.

Upon transition to a lipid-containing medium, peptides **p3** and **15c** increase their structural stability by expanding interactions between the aromatic side chains and the backbone. Interestingly, while in the presence of liposomes mimicking mammalian membrane, the backbone-backbone contacts remain unchanged, the H^N-H^N contacts extend across the entire backbone in liposomes mimicking bacterial membrane. The backbone H^N atoms of Arg2 and Arg 4 of **p3** and arg4 of **15c** show multiple NOE contacts with side chains and backbone H^Ns of "distant" residues (Figures 8E and F). This distinct behavior clearly shows the greater structural stability of **p3** and **15c** in the presence of bacterial-mimicking lipids than in water or in mammalian-mimicking liposomes.

NMR studies revealed two major structural differences between the lead peptide **15c** and its parent peptides **p3** and **p1** (the latter exhibiting higher hemolytic activity): (1) **15c** exhibited the lowest tendency to aggregate in water, and (2) it maintained the highest backbone stability. In contrast, parent peptide **p1** formed high-order oligomers or aggregates in water at concentrations above 0.15 mM due to its extensive continuous hydrophobic surface. Conversely, peptides **p3** and **15c** predominantly remained monomeric or low-oligomeric even at 1.5 mM, consistent with their fragmented hydrophobic surfaces and lower values of the molecular hydrophobicity potential (MHP) compared to parent peptide **p1** (Figure 9).

Detailed analysis of the stability/flexibility of the backbone structure in these peptides indicated another substantial difference. Since the maximal distance between neighboring backbone H^N atoms in a short cyclic peptide is almost always within the limits of NOE detectability (i.e. below 5.5 Å), the appearance of the NOE cross-peaks between them is rather defined by the structural stability of the backbone than the distances themselves. H^N groups of the backbone lacking a preferred conformation are subject to variable chemical environments. This variability arises from backbone flexibility, non-systematic aggregation via hydrophobic surfaces, and the dynamic orientations of aromatic side chains relative to the backbone. Different chemical environments, in turn, contribute to fluctuations of H^N chemical shifts, effectively "diluting" the information about NOE effect.

Taking into consideration these factors contributing to NOE signals, we can conclude that peptide **15c** with continuous NOE contacts between H^N backbone atoms of Arg1-Arg2 and arg4-dip5 has more structured backbone than **p3** (which has a single NOE contact between H^N backbone atoms of Arg1-Arg2 only) and **p1** (which shows no NOE contacts between H^N backbone atoms detected in water). Therefore, we can hypothesize that in water, both **15c** and **p3** adopts preferred, highly populated conformations with restricted backbone mobility, whereas **p1** lacks a defined conformation or its major conformation does not sufficiently constrain the orientation of the aromatic side chains, likely due to its non-systematic aggregation. Furthermore, as shown by the extended networks of cross-peaks in the NOESY spectra (Figure 8), the structures of **p3** and **15c** become even more stabilized upon interaction with bacterial membrane-mimic lipids, while this stabilization is not observed with mammalian membrane-mimics.

2.11. Molecular Dynamics analysis

The main goal of our modeling studies was to explain, at the molecular level, why in some cases, L/D isomerization of a few residues in previously designed cyclic AMPs can significantly improve the pharmacological profile of the peptides by reducing their hemolytic activity without changing antimicrobial properties. We utilized all-atom MD simulations of the peptides, followed by analyses of their structural dynamics and hydrophobic properties, to perform a comparative structure-activity analysis among the previously reported parent peptides and newly designed macrocyclic peptides containing varying numbers of D-amino acids.

Based on structural differences and hemolytic activity, we selected peptides from Series 1 and Series 3 and studied them as two individual sets having their respective parent peptides in each set. Set 1 comprised parent peptide **p1**[30] and new peptides **5a**, **7a**, and **8a**, while set 2 included parent peptide **p3**[32] and new peptides **13c**, **15c**, **16c**, and **8c** (Figure 1 and Table S3). In both sets, peptides with partial D-substitutions (e.g., **7a**, **15c**, **16c)** showed an improved hemolytic activity profile compared to their respective parent peptides (**p1** and **p3**). Conversely, not only both full D-analogs but also some alternative variants of partial D-mutants (e.g., **5a**, **13c**) showed high hemolytic activity comparable to that of their parent peptides (**p1**). These findings underscore the critical role of selective D-amino acid substitutions in modulating the balance between antimicrobial efficacy and hemolytic activity.

In the initial stage, to probe the relationship between their hemolytic activity and conformational / hydrophobic properties, the peptides were subjected to extensive MD simulations in water. Particular attention was paid to the conformational mobility of the peptides and the size/integrity of their surface hydrophobic pattern. In addition, to delineate the possible changes in membrane binding properties of a pair of peptides, we performed MD simulations of **p1** and **7a** (differ only one L/D-mutation of Arg1) in DOPC/DOPG and DOPC bilayers which mimic bacterial and mammalian cell membranes, respectively. As previously described[30], key parameters of protein-membrane binding, such as the membrane-bound modes and their populations, membrane insertion depth, and peptide-membrane contacts, were analyzed and compared.

2.11.1. Backbone flexibility and preferred conformations of the peptides in solution

Analysis of the accumulated MD ensemble revealed variations in conformational mobility in both sets of mutant peptides compared to the parent ones. The average pairwise root-mean-square deviation (RMSD) values for the backbone atoms of peptides in set 1 and set 2 ranged from 0.9–1.4 and 1.0–1.2 Å, respectively (Table S6, Supporting Information). In our previous study[32], as compared to higher hemolytic parent peptide **p1** (average RMSD value is 1.0 Å), we observed higher flexibility for less hemolytic parent peptide **p3 (**average RMSD value is 1.2 Å).

Among all the tested peptides, **8a** and **8c** (composed of all D- amino acids) demonstrated high hemolytic activity comparable to parent peptide **p1** and showed the highest flexibility (RMSD values of 1.2 and 1.4 Å, respectively). In contrast, the least toxic lead peptides, **15c** and **16c**, showed slightly lower conformational mobility during MD compared to their parent analog, **p3** (Table S6, Supporting Information). Overall, these findings point towards a complex relation between conformational mobility and hemolytic activity in the tested cyclic peptides, and therefore, a more detailed conformational analysis is required.

MD simulations revealed that the peptides change their starting configuration and form different backbone turns, defined by the proximity of the Cα atoms of residues *i* and *i+3* (cutoff distance ≤ 7Å). It was found that the populations of some of the turns correlate well with the hemolytic activity (Table S7, Supporting Information). Noticeably, the high mobility of all D-isomers (**8a**, **8c**) leads to a nearly uniform population of most of the turn populations.

Two types of backbone conformations were identified based on the C_α-C_α distance for atoms of Arg1 and Arg4, flanking the hydrophobic region. The first one contains a turn between

these residues (named "*fold1-4*") and features a turn between the polar Arg1 and Arg4, spatially separating the polar (Arg1-Arg4) and apolar (Dip5-Dip7) regions (Figure 9). The alternative backbone configuration, termed as "*fold2-6*", is characterized by an increased (> 8 Å) distance between C_α atoms of Arg1 and Arg4 and includes a different set of turns (among which the most common turn is Arg2– Dip6/Trp6, see Table S8, Supporting Information). The population distributions of these conformations correlate well with the hemolytic data across the entire set of the tested peptides (Table S7, Supporting Information). It was shown that the two sets differ markedly in the occupancy of states with *fold1-4* conformation.

In Dip6-containing peptides (set 1), this backbone conformation is either nearly absent (e.g., **p1**, **5a**, and **7a**) or constitutes only a minor population for highly flexible peptides, such as **8a** (Table S6, Supporting Information). In contrast, *fold1-4* is well populated, or even the dominant conformation), in all Trp6-containing peptides (**p3** and **15c**) from set 2.

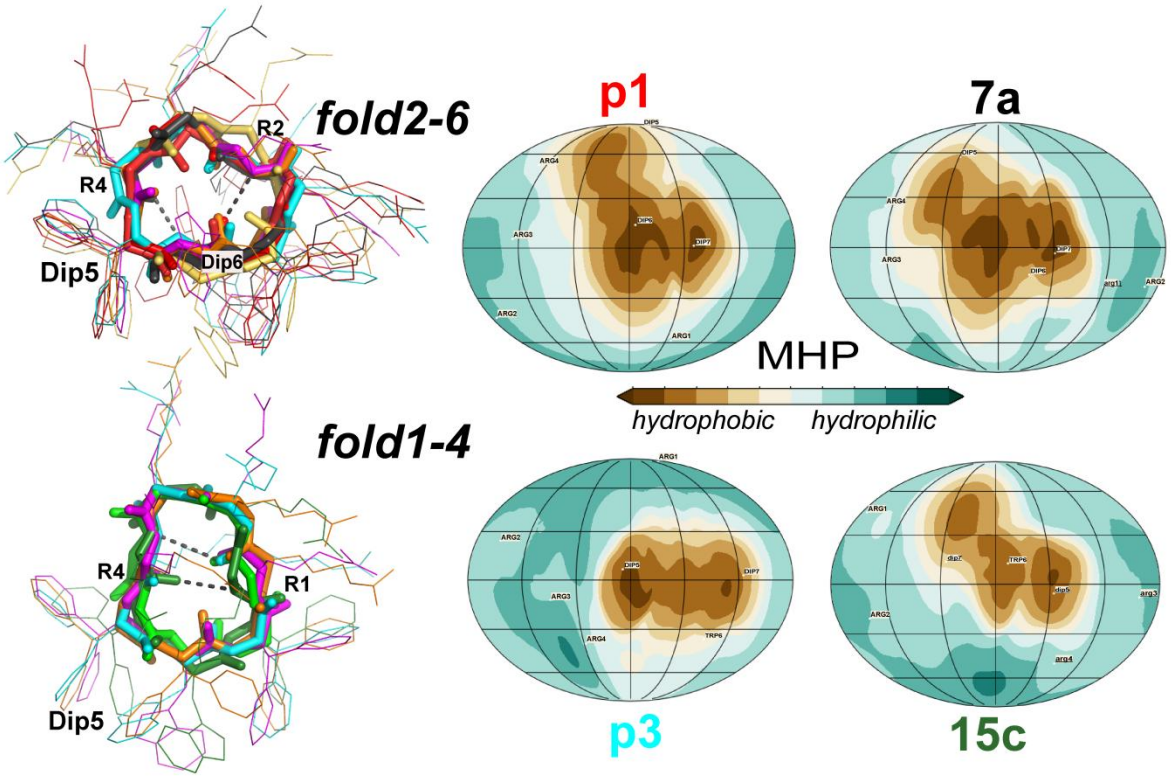

Figure 9. Principal conformational states of the peptides and distribution of MHP on their surfaces. (Left) Spatial structures in stick mode represent the most-populated conformations of the peptides in water. The most common hydrogen bonds (dashed lines) and residues involved (residue numbers) are shown. (Right) MD-averaged MHP spherical projection maps are displayed for the most populated MD-states in both fold types. Structures and MHP maps for the peptides in *fold2-6* and *fold1-4* conformations are shown on the top and bottom, respectively. Peptide-induced MHP values on the peptide molecular surface are color-coded

according to the scale bar. Peptide names and corresponding 3D structures are in the same color.

The states with *fold2-6* are prevalent in set 1 peptides (**p1**, **5a**, **7a**, and **8a**) but are less populated in set 2 peptides (**p3**, **8c**, **13c**, **15c**, and **16c**). This variation in conformational populations reflects changes in the side chain packing arising from both Dip6/Trp6 and L/D substitutions in the parent peptides. In peptides with a higher population of *fold2-6* MD states, we found denser molecular packing characterized by a higher number of backbone H-bonds and more stable π-cationic and stacking interactions between the side chains of adjacent Arg and Dip residues (Arg1-Dip7, Arg4-Dip5, Table S6, Supporting Information).

All designed cyclic membrane-active peptides have clearly amphiphilic nature, with well-defined surface regions: hydrophilic (residues 1-4) and hydrophobic (residues 5–7). As shown in our previous work[32], the replacement of the bulky Dip side chain with a flat aromatic Trp side chain (its surface area is approximately 15% smaller) elevates the conformational mobility and decreases the integrity of the apolar motif in peptide **p3**. Indeed, all Trp6-containing peptides in set 2 show diminished integrity of their apolar motifs (Figure S1, Supporting Information), leading to increased solvent accessibility of the polar backbone atoms within residues that form the hydrophobic pattern (Table S6, Supporting Information).

Summarizing the MD data, the peptides from different sets demonstrate distinct differences in the size and shape of their hydrophobic patterns (Figure S1, Supporting Information). Peptides in set 1, characterized by the bulky Dip6 side chain, display a larger non-polar surface, higher surface MHP values, and greater hydrophobic surface integrity (continuous areas of high MHP values). Most of them are highly toxic, with an HC_{50} ranging between ~45-70 μg/mL). In contrast, Trp6-containing peptides from set 2 exhibit reduced hydrophobicity and variability in hemolytic activity. Compared to the low-hemolytic lead peptides **15c** and **16c**, peptides **8c** and **13c** have more consolidated hydrophobic surfaces with elevated MHP values (Figure S1, Supporting Information).

In conclusion, irrespective of the parent peptide, the less toxic D-mutants generally exhibit smaller and more fragmented hydrophobic surface patches. Variations in side-chain packing, driven by L/D or amino acid substitutions, result in distinct populations of backbone conformations. Peptides with high hemolytic activity (e.g., **p1**, **5a**, **8a**, **13c**) predominantly adopt *fold2-6* states, while those with low hemolytic activity (e.g., **p3**, **15c**, **16c**) are primarily associated with *fold1-4* states. Thus, there is a relationship between backbone conformation and hemolytic behaviour in the peptide sets.

The conformational flexibility of peptides composed entirely of D-amino acids (e.g., **8a** and **8c**, Table S7, Supporting Information) can facilitate the adaptation of the peptides to the membrane environment and their incorporation into the membrane. In contrast, a minor modification, such as the single-residue D-stereoisomer **7a** compared to the parent **p1**, does not result in sufficient changes in the distribution of surface hydrophobic properties and/or backbone conformations, as anticipated. In summary, predicting toxicity changes solely based on surface hydrophobicity mapping and/or backbone conformation populations appears highly challenging (Figure S1, Table S6, Supporting Information).

2.7.2 Spatial organization of the hydrophobic pattern

A more detailed analysis of the hydrophobic region of the peptides revealed different variants of packing of the flanking side chains of Dip residues 5 and 7, categorized as either non-contacting or closely packed. These two states have rather extended (named as "*flat*") or more curved ("*bend*") backbone conformation of the apolar region (Figure 10). To distinguish these two modes of packing in the apolar region, we used the distance cutoff of 8 Å between any heavy atoms of the side chains of residues Dip5 and Dip7. No contacts between these side chains within the cutoff were detected for the "*flat*" conformation, whereas in the "*bend"* state, side chains of the flanking hydrophobic residues have at least one atom-atom distance that falls within the 8 Å threshold.

Thus, despite the overall similarity in backbone conformation distribution in **p1** and **7a** (*fold1-4* is practically absent in both peptides, Table S6, Supporting Information), notable differences appear at the level of spatial organization of their hydrophobic side chains. The *flat* state is weakly populated for **p1** and becomes the dominant conformation for **7a** (Table S9, Supporting Information). We also found a strong correlation between "*flat*" and "*bend*" conformations of the hydrophobic pattern and the range of the dihedral angle φ of Dip6 in **p1** and **7a** (Figure 10D). In the *flat* state, most of the peptides exhibit an increase in the overall solvent exposure of the backbone atoms of hydrophobic residues (Table S9, Supporting Information). As a result, the *flat*–organized hydrophobic region of a peptide may be less effective in deep membrane insertion due to the reduced complementarity of the peptide surface with the hydrophobic environment of the membrane. Indeed, in contrast to other peptides from set 1 (**p1, 5a**, **8a)** that have low occupancy of flat conformations and high hemolytic action, **7a** is obviously less cytotoxic (Figure 2 and Table S3, Supporting Information).

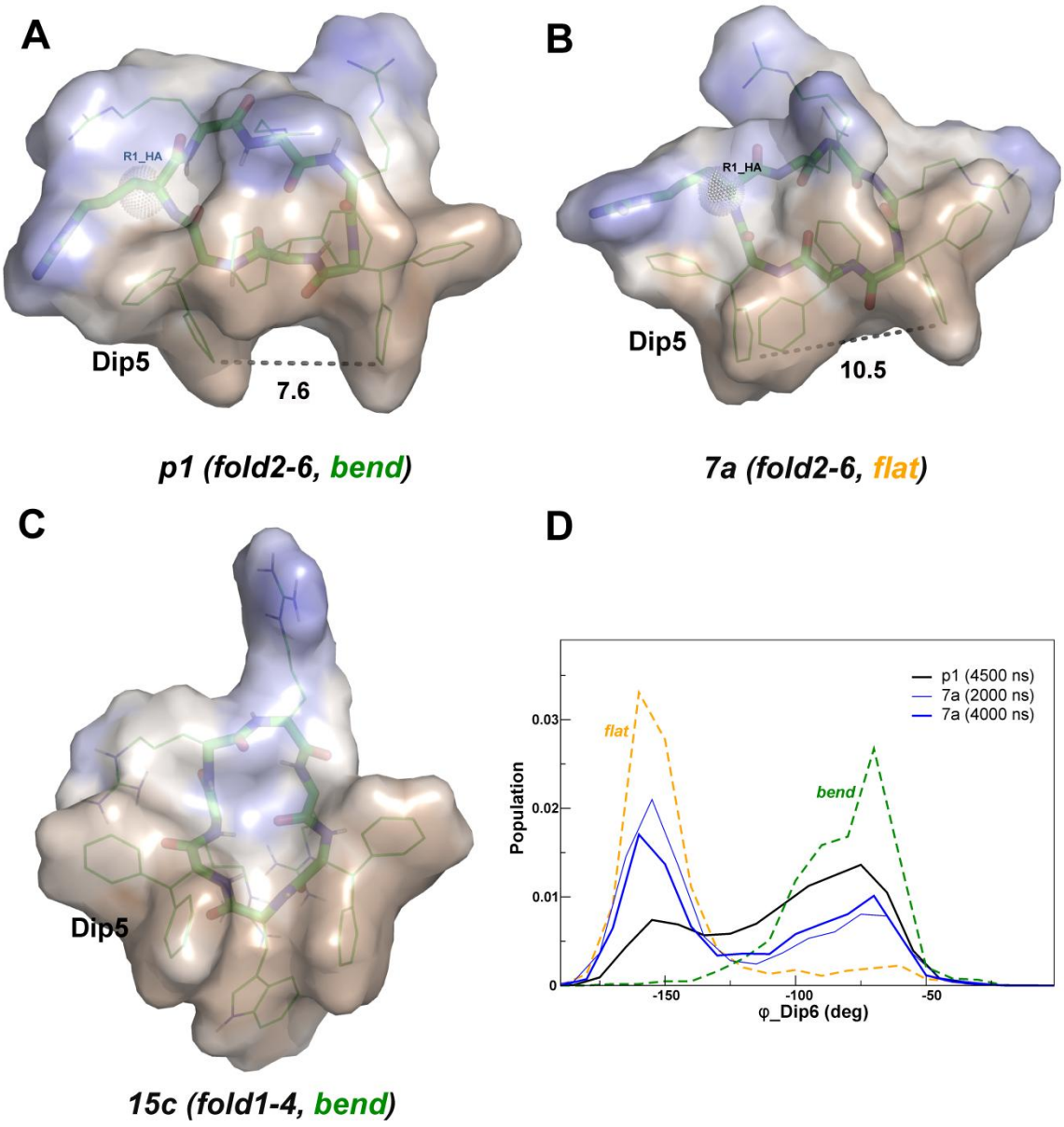

Figure 10. Organization of the hydrophobic pattern for peptides **p1**, **7a**, and **15c** in aqueous environment. Preferred backbone conformations of peptides **p1** (A, parent) and **7a** (B, having D-isomer of Arg1, stereoisomeric substitution is indicated by the location of R1_HA atom), and the lead cyclic peptide **15c** (C). Peptides **p1** (A) and **7a** (B) have very similar *fold2-6* conformations with an elongated hydrophobic patch, compared with alternative *fold1-4* conformation of peptide **15c** (C). Molecular surfaces of the peptides in *bend* (A, C) and *flat* (B) conformations, with surfaces color-coded based on molecular hydrophobicity potential (MHP) values: blue for hydrophilic regions and brown for hydrophobic regions. (D) Normalized histograms of distributions of dihedral angle φ of Dip6. The association of two major peaks with the different geometry of the apolar pattern (*flat* or *bend*) is demonstrated by dash lines indicating the distribution of φ of Dip6 in *flat* and *bend* populations of the peptide.

2.7.3 Membrane binding

To elucidate the potential differences in membrane-binding properties of a pair of the peptides with the same sequence and single L/D substitution of Arg1, the parent peptide **p1** and less cytotoxic **7a**, a series of MD simulations in a water-membrane environment was performed. The model membrane mimicking the mammalian cells was represented by a DOPC lipid bilayer. In addition, MD simulation of peptide **7a** was carried out in the presence of a two-component bilayer DOPC/DOPG (with a molar ratio of 7.5/2.5) mimicking a bacterial membrane.

As shown earlier[30], interaction with the bilayer significantly restricts the conformational mobility of the cyclic peptides compared to that in water. Regardless of the starting model - *flat* or *bend* conformations found in water - binding to the membrane did not induce significant changes in the spatial structure (the average RMSD values of the backbone atoms are ~0.5 Å). Similar to other cyclic AMP peptides analyzed[30, 34], the most populated membrane-bound mode, the peptides interact with the lipid polar head groups through the Arg residues, while the peptide's hydrophobic motif is oriented toward the solvent (named earlier as mode "UP" or "*polar*"). Compared to UP-mode, membrane binding through apolar residues (*apolar* mode) is characterized by a larger contact area and a smaller distance between the peptide center of the mass and the bilayer center.

Regardless of the type of lipid bilayer, both peptides **7a** and **p1** have similar distributions in terms of lipid contact area and insertion depth (Figure S2, Supporting Information). It is interesting to note that the partially inserted states (only 1-2 apolar residues embedded in the membrane) are more populated for **7a** in both DOPC (10% compared to <1% for **p1**) and DOPC/DOPG bilayers (7% versus 4% for **p1**). Both conformations (*flat* and *bend*) observed for the peptides in water were effective for insertion into the lipid acyl core of the membrane.

It is worth noting that in the successful MD runs started from *flat* conformations of the peptides and resulting in *apolar* mode (especially in the case of DOPC/DOPG bilayer), an increase of *bend*-state population was more pronounced and associated with the insertion process (Figure S3, Supporting Information). MD analysis provided insights into the conformational space of the peptides in water, their hydrophobic surface behavior, and the relationship between these features and their biological properties. Multiple independent MD calculations in an aqueous environment showed conformational variability of all tested peptides, which is consistent with the NMR data obtained for **p1**, **p3** and **15c**. In set 2, the least toxic lead peptides (**15c** and **16c**) were also found to be less flexible compared to the parent

p3. At the same time, the more stable peptides, **5a** and **13c**, exhibited higher toxicity than their flexible parent peptides. Additionally, increased flexibility observed for the highly hemolytic peptides **8a** and **8c** - full D-analogues of **p1** and **p3** - suggests that flexibility may contribute significantly to peptide toxicity.

Computational analysis of the conformational behavior of representative peptides identified four distinct backbone conformations, each associated with the membrane-binding properties of the peptides. Two of them, *fold1-4* and *fold2-6*, determine the general shape of the molecule backbone, while the other two, *flat* and *bend*, characterize the shape and plasticity of the surface hydrophobic patch formed by both the backbone and side chains. Depending on the population ratio within the types of these conformations, each cyclic peptide can be classified into one of four classes, as shown in Figure 11.

This classification correlates with the hemolytic activity of the peptides. Compared to *fold1-4*/*flat* conformations, peptides in the *fold2-6*/*bend* class are expected to have better surface complementarity to the hydrophobic membrane environments, resulting in stronger hemolytic properties. Conversely, peptides with *fold1-4/flat* conformations are likely to have reduced hemolytic activity. X and Y axes define the *fold2-6/fold1-4* and *bend/flat* population, ratios, respectively. Indeed, as can be seen from Figure 11, all peptides with high hemolytic activity (**p1**, **5a**, **8a**, **13c**) are clustered on the right side of the diagram (mostly in the upper-right quadrant, where both *fold2-6/fold1-4* and *bend/flat* population ratios exceed 1. In contrast, the less toxic peptides **p3**, **15c**, **16c** or **7a** are positioned in the upper-left ($X < 1$, $Y > 1$) or lower-right ($X > 1$, $Y < 1$) quadrants.

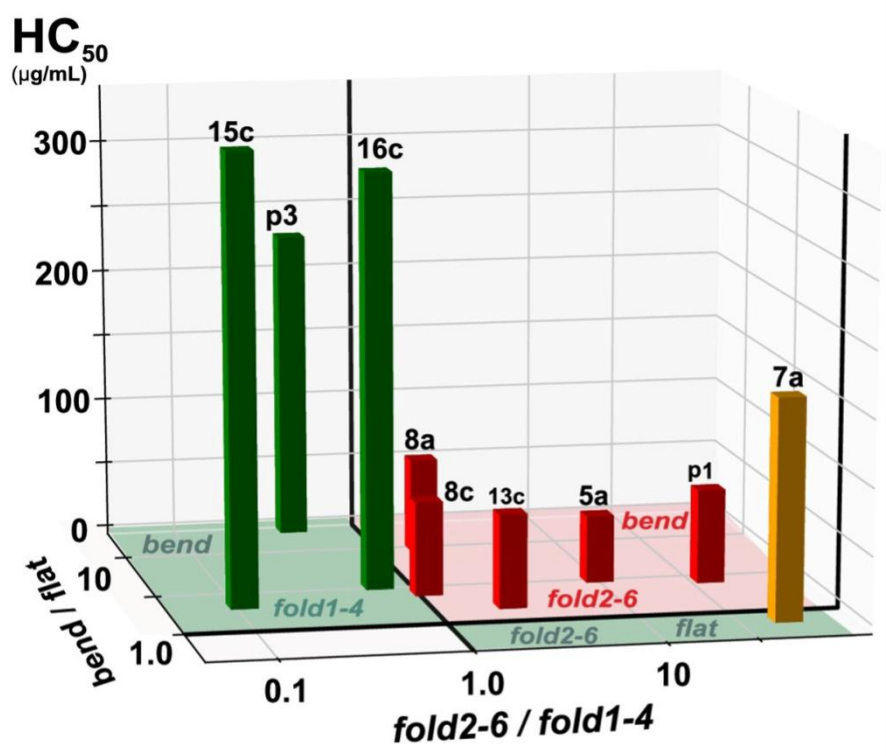

Figure 11. Hemolytic activity (HC_{50}) of the studied peptides and their attribution to one of four conformational/hydrophobicity types based on the population ratios of MD-derived backbone configurations. Peptides are color-coded to indicate their levels of hemolytic activity: red for high, brown for medium, and green for low activity. Ration values on the X and Y axes are given in a logarithmic scale.

3. CONCLUSIONS

We successfully synthesized a library of macrocyclic peptides and examined the impact of stereochemical replacements on the antimicrobial activity and cytotoxicity. Detailed analysis of the data revealed that partial or complete stereochemical substitution resulted in minimal changes in antimicrobial activity but significantly reduced cytotoxicity compared to the parent peptides. For instance, lead peptides **15c** and **16c** displayed similar or slightly higher MICs (1-fold increase) against all the tested bacterial strains compared to the parent **p3**. Despite retaining comparable antimicrobial potency, **15c** and **16c** exhibited substantially improved microbial selectivity over mammalian cells, as indicated by a higher therapeutic index. Time-dependent killing and antibiofilm assays confirmed their membrane-disruptive properties, supported by calcein dye leakage and SEM imaging data. Furthermore, neither wild-type nor antibiotic-resistant strains of *S. aureus* and *E. coli* exhibited resistance to **15c** or **16c**, suggesting a multifaceted mode of action akin to naturally occurring AMPs. As expected, given the

presence of multiple non-proteogenic amino acids, including D-isomers in a cyclic framework, both **15c** and **16c** showed good plasma stability with $t_{1/2}$ of 6 h and 8 h, respectively.

A comprehensive understanding of peptide behavior required a combination of experimental techniques (e.g., NMR) and computational methods (e.g., MD simulations, MHP mapping). Their application to the most potent peptides and corresponding analogs provided insights into structural differences that influence their biological profiles, including peptide conformation, flexibility, surface amphiphilicity, and oligomerization tendencies. In summary, it can be assumed with some confidence that peptides with limited flexibility and side-chain packing that creates a smaller, more fragmented surface hydrophobic pattern are less likely to insert into eukaryotic membranes, thereby exhibiting reduced toxicity. The key finding of this study is that the hemolytic activity of cyclic amphiphilic peptides (at least within the current extensive dataset) can be reliably predicted by considering the nuanced interplay of structural and hydrophobic parameters derived from computer simulations guided by NMR data. Notably, the proposed SAR model is inherently multifactorial. No single parameter, such as flexibility, backbone conformation type, side-chain packing density, or polar backbone accessibility, alone predicts hemolytic activity. Instead, the combination of these factors defines the activity profile. This SAR model offers a valuable framework for the rational design of related peptides or peptidomimetics, enabling the development of compounds with tailored pharmacological profiles.

4. EXPERIMENTAL SECTION

4.1. Materials

2-Chlorotrityl chloride resin (loading 0.572 mmol/g) was purchased from Sigma-Aldrich (St. Louis, MO, USA). The coupling reagent 2-(1H-benzotriazole-1-yl)-1,1,3,3-tetramethylaminium hexafluorophosphate (HBTU), and building block amino acids Fmoc-L-Arg(Pbf)-OH, Fmoc-D-Arg(Pbf)-OH, Fmoc-L-Trp(Boc)-OH, and Fmoc-D-Trp(Boc)-OH were purchased from AAPPTec LLC (Louisville, KY, USA). Unnatural amino acids Fmoc-L-Ala(3,3-diphenyl)-OH, Fmoc-D-Ala(3,3-diphenyl)-OH, Fmoc-L-Ala(1-naphthyl)-OH, and Fmoc-D-Ala(1-naphthyl)-OH were purchased from Chem-Impex International Inc. (Wood Dale, IL, USA). *N*,*N*-Dimethylformamide (DMF), dichloromethane (DCM), *N*,*N*-diisopropylethylamine (DIPEA), trifluoroethanol (TFE), trifluoroacetic acid (TFA), triisoproylsilane (TIS), piperidine, and all other reagents were bought from Sigma-Aldrich (St. Louis, MO, USA). 1-Hydroxy-7-azabenzotriazole (HOAt), 1-hydroxybenzotriazole (HOBt),

and 1,3-diisopropylcarbodiimide (DIC) were purchased from Sigma-Aldrich Chemical Co. (Milwaukee, WI, USA). Ultra-pure water was purchased from the Milli-Q system (Temecula, CA, USA). MTS assay kit (98%) was purchased from Promega (Madison, WI, USA). Single donor human Plasma K2 EDTA was purchased from Innov-Research (Novi, MI, USA). All phospholipids and cholesterol were purchased from Avanti polar Lipids (Alabaster, USA). Calcein dye was obtained from Sigma.

All the mammalian and bacterial cell culture supplies were purchased from Corning (Christiansburg, VA, USA) and Fisher Scientific (Waltham, MA, USA). All the mammalian and bacterial cell experiments were carried out under a laminar flow hood Labconco (Kansas City, MO, USA). Cell culture was carried out at 37 °C with 5% CO_2 in a Forma incubator using a T-75 flask. The human lung fibroblast cell (MRC-5, ATCC No. CCL-171), human embryonic kidney cells (HEK293, ATCC No. CRL 1573), and human hepatoma HepaRG cells (Gibco, HPRGC10) were purchased from ATCC (USA). All cells were maintained in a 5% CO_2 incubator (37 °C). Human serum was purchased from Sigma-Aldrich. All bacterial strains employed in this study are procured from VWR, USA, and propagated as per the recommendation of the American Type Culture Collection (ATCC). The strains with their classification and properties are listed in Table S2 (Supporting Information).

4.2. Solid-phase peptide synthesis and macrocyclization

All the peptides were synthesized manually on 2-chlorotrityl chloride resin by employing standard Fmoc/tBu solid-phase peptide synthesis protocol. Fmoc-L-amino acid or Fmoc-D-amino acid building blocks were coupled to the resin using the HBTU, HOBt, and DIPEA in DMF. Fmoc protecting groups were removed by treatment with 20% (v/v) piperidine in DMF after each coupling. After the complete extension of the desired peptide sequence, the side chain-protected peptides were detached from the resin by treating the peptidyl resin with a mixture of TFE/acetic acid/DCM [2:1:7 (v/v/v)]. The crude-protected peptides were separated by filtration from the resin and precipitated with chilled diethyl ether. The crude masses of protected peptides were dried under vacuum and cyclized using HOAt and DIC in an anhydrous DMF/DCM [1:4 (v/v)] mixture. Following the head-to-tail cyclization, the protecting groups were removed with a cocktail of TFA/water/TIS [95:2.5:2.5 (v/v/v)], and the crude peptide was precipitated with ice-cooled diethyl ether. After multiple ether washes, the obtained crude mass was redissolved in acetonitrile/water (1:1 v/v with 0.5% TFA), and the solution was lyophilized to obtain the crude peptide.

4.3. Purification and analytical characterization of peptides

The crude cyclic peptides were purified using a reversed-phase high-pressure liquid chromatography (RP-HPLC) system (Shimadzu LC-20AP). Peptides were dissolved in acetonitrile/water (1:2 v/v, with 0.5% TFA) to a final concentration of 10-12 mg/mL. Following filtration through 0.45 µm Millipore filter the peptide solutions were loaded on to column via multiple 5 mL injections. Preparative C18 column (Gemini, 5 µm particle size, 100 Å pore size, 21.2 mm × 250 mm) from Phenomenex was used with a mixture of water and acetonitrile (both containing 0.1% (v/v) TFA) as eluent at a flow rate of 10 mL/min. The detection wavelength was 220 nm. Fractions containing the desired peptides were lyophilized.

The purity analysis of the peptides was conducted on RP-HPLC system Prominence-i (Shimadzu Corp., Kyoto, Japan) by using an analytical Delta-Pak (Waters) C18 column (100 Å, 5 µm, 3.9 mm × 150 mm). The mass of the purified peptides was determined in positive ion mode using EVOQ Triple Quadrupole LC-TQ (Q-Tof, Bruker, USA). The purity (>95%) and high-resolution mass data of all cyclic peptides and their linear analogs have been provided as supporting information.

Series 1: 1a c[Arg-Arg-Arg-Arg-Dip-Dip-**dip**]: HR-MS (ESI-TOF) (m/z) $C_{69}H_{87}N_{19}O_7$ calcd: 1293.7036; found, 1294.9723 $[M+H]^+$, 1408.7172 $[M+TFA]^+$, 647.8704 $[M+H]^{2+}$, 432.2261 $[M+H]^{3+}$; **2a** c[Arg-Arg-Arg-Arg-Dip-**dip**-Dip]: HR-MS (ESI-TOF) (m/z) $C_{69}H_{87}N_{19}O_7$ calcd: 1293.7036; found, 1294.7219 $[M+H]^+$, 647.8695 $[M+H]^{2+}$, 470.2501 $[M+TFA]^{3+}$; **3a** c[Arg-Arg-Arg-Arg-**dip**-Dip-Dip]: HR-MS (ESI-TOF) (m/z) $C_{69}H_{87}N_{19}O_7$ calcd: 1293.7036; found, 1294.7245 $[M+H]^+$, 1408.7183 $[M+TFA]^+$, 647.8705 $[M+H]^{2+}$, 432.2126 $[M+H]^{3+}$; **4a** c[Arg-Arg-Arg-**arg**-Dip-Dip-Dip]: HR-MS (ESI-TOF) (m/z) $C_{69}H_{87}N_{19}O_7$ calcd: 1293.7036; found, 1294.8726 $[M+H]^+$, 1408.7206 $[M+TFA]^+$, 647.8715 $[M+H]^{2+}$; **5a** c[Arg-Arg-**arg**-Arg-Dip-Dip-Dip]: HR-MS (ESI-TOF) (m/z) $C_{69}H_{87}N_{19}O_7$ calcd: 1293.7036; found, 1294.6727 $[M+H]^+$, 647.8714 $[M+H]^{2+}$, 432.2625 $[M+H]^{3+}$; **6a** c[Arg-**arg**-Arg-Arg-Dip-Dip-Dip]: HR-MS (ESI-TOF) (m/z) $C_{69}H_{87}N_{19}O_7$ calcd: 1293.7036; found, 1294.7263 $[M+H]^+$, 1408.7196 $[M+TFA]^+$, 647.8709 $[M+H]^{2+}$, 470.2631 $[M+TFA]^{3+}$; **7a** c[**arg**-Arg-Arg-Arg-Dip-Dip-Dip]: HR-MS (ESI-TOF) (m/z) $C_{69}H_{87}N_{19}O_7$ calcd: 1293.7036; found, 1294.6726 $[M+H]^+$, 1408.7203 $[M+TFA]^+$, 647.8712 $[M+H]^{2+}$; **8a** c[**arg-arg-arg-arg-dip-dip-dip**]: HR-MS (ESI-TOF) (m/z) $C_{69}H_{87}N_{19}O_7$ calcd: 1293.7036; found, 1294.7356 $[M+H]^+$, 647.8717 $[M+H]^{2+}$, 432.2663 $[M+H]^{3+}$; **9a** c[Arg-Arg-Arg-Arg-**dip-dip-dip**]: HR-MS (ESI-TOF) (m/z) $C_{69}H_{87}N_{19}O_7$ calcd: 1293.7036; found, 1294.7320 $[M+H]^+$, 647.8698 $[M+H]^{2+}$; **10a** c[**arg-arg-arg-arg**-Dip-Dip-Dip]: HR-MS (ESI-TOF) (m/z) $C_{69}H_{87}N_{19}O_7$ calcd: 1293.7036; found,

1294.8724 $[M+H]^+$, 648.3702 $[M+H]^{2+}$; **11a** c[**arg**-Arg-**arg**-Arg-**dip-dip-dip**]: HR-MS (ESI-TOF) (m/z) $C_{69}H_{87}N_{19}O_7$ calcd: 1293.7036; found, 1294.7271 $[M+H]^+$, 647.8715 $[M+H]^{2+}$, 432.2155 $[M+H]^{3+}$; **12a** c[Arg-**arg**-Arg-**arg-dip-dip-dip**]: HR-MS (ESI-TOF) (m/z) $C_{69}H_{87}N_{19}O_7$ calcd: 1293.7036; found, 1294.7227 $[M+H]^+$, 1408.7161 $[M+TFA]^+$, 647.8690 $[M+H]^{2+}$; **13a** c[**arg**-Arg-**arg**-Arg-**dip**-Dip-**dip**]: HR-MS (ESI-TOF) (m/z) $C_{69}H_{87}N_{19}O_7$ calcd: 1293.7036; found, 1294.7824 $[M+H]^+$, 648.3270 $[M+H]^{2+}$; **14a** c[Arg-**arg**-Arg-**arg**-Dip-**dip**-Dip]: HR-MS (ESI-TOF) (m/z) $C_{69}H_{87}N_{19}O_7$ calcd: 1293.7036; found, 1294.7305 $[M+H]^+$, 1408.7240 $[M+TFA]^+$, 647.8728 $[M+H]^{2+}$; **15a** c[Arg-Arg-**arg-arg-dip-dip-dip**]: HR-MS (ESI-TOF) (m/z) $C_{69}H_{87}N_{19}O_7$ calcd: 1293.7036; found, 1294.7293 $[M+H]^+$, 647.8725 $[M+H]^{2+}$; **16a** c[**arg-arg**-Arg-Arg-**dip-dip-dip**]: HR-MS (ESI-TOF) (m/z) $C_{69}H_{87}N_{19}O_7$ calcd: 1293.7036; found, 1294.7293 $[M+H]^+$, 647.8716 $[M+H]^{2+}$, 432.2612 $[M+H]^{3+}$;

Series 2: 1b c[Arg-Arg-Arg-Arg-Nal-Nal-**nal**]: HR-MS (ESI-TOF) (m/z) $C_{63}H_{81}N_{19}O_7$ calcd: 1215.6566; found, 1216.6802 $[M+H]^+$, 608.8495 $[M+H]^{2+}$; **2b** c[Arg-Arg-Arg-Arg-Nal-**nal**-Nal]: HR-MS (ESI-TOF) (m/z) $C_{63}H_{81}N_{19}O_7$ calcd: 1215.6566; found, 1216.6810 $[M+H]^+$, 608.8499 $[M+H]^{2+}$; **3b** c[Arg-Arg-Arg-Arg-**nal**-Nal-Nal]: HR-MS (ESI-TOF) (m/z) $C_{63}H_{81}N_{19}O_7$ calcd: 1215.6566; found, 1216.7886 $[M+H]^+$, 1330.7736 $[M+TFA]^+$, 608.8485 $[M+H]^{2+}$; **4b** c[Arg-Arg-Arg-**arg**-Nal-Nal-Nal]: HR-MS (ESI-TOF) (m/z) $C_{63}H_{81}N_{19}O_7$ calcd: 1215.6566; found, 1216.6798 $[M+H]^+$, 1330.8777 $[M+TFA]^+$, 608.8488 $[M+H]^{2+}$; **5b** c[Arg-Arg-**arg**-Arg-Nal-Nal-Nal]: HR-MS (ESI-TOF) (m/z) $C_{63}H_{81}N_{19}O_7$ calcd: 1215.6566; found, 1216.6861 $[M+H]^+$, 1330.6773 $[M+TFA]^+$, 608.8533 $[M+H]^{2+}$; **6b** c[Arg-**arg**-Arg-Arg-Nal-Nal-Nal]: HR-MS (ESI-TOF) (m/z) $C_{63}H_{81}N_{19}O_7$ calcd: 1215.6566; found, 1216.6786 $[M+H]^+$, 608.8482 $[M+H]^{2+}$; **7b** c[**arg**-Arg-Arg-Arg-Nal-Nal-Nal]: HR-MS (ESI-TOF) (m/z) $C_{63}H_{81}N_{19}O_7$ calcd: 1215.6566; found, 1216.9796 $[M+H]^+$, 608.8489 $[M+H]^{2+}$; **8b** c[**arg-arg-arg-arg-nal-nal-nal]**: HR-MS (ESI-TOF) (m/z) $C_{63}H_{81}N_{19}O_7$ calcd: 1215.6566; found, 1216.8483 $[M+H]^+$, 1330.8673 $[M+TFA]^+$, 608.8496 $[M+H]^{2+}$; **9b** c[Arg-Arg-Arg-Arg-**nal-nal-nal**]: HR-MS (ESI-TOF) (m/z) $C_{63}H_{81}N_{19}O_7$ calcd: 1215.6566; found, 1216.6780 $[M+H]^+$, 1330.8773 $[M+TFA]^+$, 608.8477 $[M+H]^{2+}$; **10b** c[**arg-arg-arg-arg**-Nal-Nal-Nal]: HR-MS (ESI-TOF) (m/z) $C_{63}H_{81}N_{19}O_7$ calcd: 1215.6566; found, 1216.9677 $[M+H]^+$, 608.8476 $[M+H]^{2+}$; **11b** c[**arg**-Arg-**arg**-Arg-**nal-nal-nal**]: HR-MS (ESI-TOF) (m/z) $C_{63}H_{81}N_{19}O_7$ calcd: 1215.6566; found, 1216.6790 $[M+H]^+$, 1330.7787 $[M+TFA]^+$, 608.8486 $[M+H]^{2+}$; **12b** c[Arg-**arg**-Arg-**arg-nal-nal-nal**]: HR-MS (ESI-TOF) (m/z) $C_{63}H_{81}N_{19}O_7$ calcd: 1215.6566; found, 1216.6771 $[M+H]^+$, 608.8474 $[M+H]^{2+}$; **13b** c[**arg**-Arg-**arg**-Arg-**nal**-Nal-**nal**]: HR-MS (ESI-TOF) (m/z) $C_{63}H_{81}N_{19}O_7$ calcd: 1215.6566; found, 1216.8682 $[M+H]^+$, 608.8503 $[M+H]^{2+}$;

14b c[Arg-**arg**-Arg-**arg**-Nal-**nal**-Nal]: HR-MS (ESI-TOF) (m/z) $C_{63}H_{81}N_{19}O_7$ calcd: 1215.6566; found, 1216.7876 $[M+H]^+$, 608.8483 $[M+H]^{2+}$; **15b** c[Arg-Arg-**arg-arg-nal-nal-nal**]: HR-MS (ESI-TOF) (m/z) $C_{63}H_{81}N_{19}O_7$ calcd: 1215.6566; found, 1216.6804 $[M+H]^+$, 608.8490 $[M+H]^{2+}$; **16b** c[**arg-arg**-Arg-Arg-**nal-nal-nal**]: HR-MS (ESI-TOF) (m/z) $C_{63}H_{81}N_{19}O_7$ calcd: 1215.6566; found, 1216.6773 $[M+H]^+$, 1330.8767 $[M+TFA]^+$, 608.8472 $[M+H]^{2+}$;

Series 3: 1c c[Arg-Arg-Arg-Arg-Dip-Trp-**dip**]: HR-MS (ESI-TOF) (m/z) $C_{65}H_{84}N_{20}O_7$ calcd: 1256.6832; found, 1257.7009 $[M+H]^+$, 629.3588 $[M+H]^{2+}$; **2c** c[Arg-Arg-Arg-Arg-Dip-**trp**-Dip]: HR-MS (ESI-TOF) (m/z) $C_{65}H_{84}N_{20}O_7$ calcd: 1256.6832; found, 1257.6293 $[M+H]^+$, 629.3596 $[M+H]^{2+}$; **3c** c[Arg-Arg-Arg-Arg-**dip**-Trp-Dip]: HR-MS (ESI-TOF) (m/z) $C_{65}H_{84}N_{20}O_7$ calcd: 1256.6832; found, 1257.7032 $[M+H]^+$, 629.3603 $[M+H]^{2+}$; **4c** c[Arg-Arg-Arg-**arg**-Dip-Trp-Dip]: HR-MS (ESI-TOF) (m/z) $C_{65}H_{84}N_{20}O_7$ calcd: 1256.6832; found, 1257.7052 $[M+H]^+$, 629.3609 $[M+H]^{2+}$; **5c** c[Arg-Arg-**arg**-Arg-Dip-Trp-Dip]: HR-MS (ESI-TOF) (m/z) $C_{65}H_{84}N_{20}O_7$ calcd: 1256.6832; found, 1257.8702 $[M+H]^+$, 629.3598 $[M+H]^{2+}$, 419.6606 $[M+H]^{3+}$; **6c** c[Arg-**arg**-Arg-Arg-Dip-Trp-Dip]: HR-MS (ESI-TOF) (m/z) $C_{65}H_{84}N_{20}O_7$ calcd: 1256.6832; found, 1257.6039 $[M+H]^+$, 629.3603 $[M+H]^{2+}$; **7c** c[**arg**-Arg-Arg-Arg-Dip-Trp-Dip]: HR-MS (ESI-TOF) (m/z) $C_{65}H_{84}N_{20}O_7$ calcd: 1256.6832; found, 1257.7703 $[M+H]^+$, 629.3598 $[M+H]^{2+}$; 419.9922 $[M+H]^{3+}$; **8c** c[**arg-arg-arg-arg**-Dip-Trp-Dip]: HR-MS (ESI-TOF) (m/z) $C_{65}H_{84}N_{20}O_7$ calcd: 1256.6832; found, 1257.7044 $[M+H]^+$, 629.3602 $[M+H]^{2+}$; **9c** c[Arg-Arg-Arg-Arg-**dip-trp-dip**]: HR-MS (ESI-TOF) (m/z) $C_{65}H_{84}N_{20}O_7$ calcd: 1256.6832; found, 1257.7104 $[M+H]^+$, 629.3599 $[M+H]^{2+}$; **10c** c[**arg-arg-arg-arg-dip-trp-dip**]: HR-MS (ESI-TOF) (m/z) $C_{65}H_{84}N_{20}O_7$ calcd: 1256.6832; found, 1257.9704 $[M+H]^+$, 629.3600 $[M+H]^{2+}$, 419.9229 $[M+H]^{3+}$; **11c** c[Arg-Arg-Arg-Arg-**dip**-Trp-**dip**]: HR-MS (ESI-TOF) (m/z) $C_{65}H_{84}N_{20}O_7$ calcd: 1256.6832; found, 1257.7088 $[M+H]^+$, 629.3632 $[M+H]^{2+}$; 419.6048 $[M+H]^{3+}$; **12c** c[**arg-arg-arg-arg-dip**-Trp-**dip**]: HR-MS (ESI-TOF) (m/z) $C_{65}H_{84}N_{20}O_7$ calcd: 1256.6832; found, 1257.8063 $[M+H]^+$, 629.3621 $[M+H]^{2+}$, 419.7205 $[M+H]^{3+}$; **13c** c[**arg**-Arg-**arg**-Arg-**dip**-Trp-**dip**]: HR-MS (ESI-TOF) (m/z) $C_{65}H_{84}N_{20}O_7$ calcd: 1256.6832; found, 1257.7077 $[M+H]^+$, 629.3626 $[M+H]^{2+}$; 419.6066 $[M+H]^{3+}$; **14c** c[Arg-**arg**-Arg-**arg-dip**-Trp-**dip**]: HR-MS (ESI-TOF) (m/z) $C_{65}H_{84}N_{20}O_7$ calcd: 1256.6832; found, 1257.8702 $[M+H]^+$, 629.3595 $[M+H]^{2+}$; 419.7776 $[M+H]^{3+}$; **15c** c[Arg-Arg-**arg-arg- dip**-Trp-**dip**]: HR-MS (ESI-TOF) (m/z) $C_{65}H_{84}N_{20}O_7$ calcd: 1256.6832; found, 1257.7330 $[M+H]^+$, 629.3602 $[M+H]^{2+}$; 419.7266 $[M+H]^{3+}$; **16c** c[**arg-arg**-Arg-Arg- **dip**-Trp-**dip**]: HR-MS (ESI-TOF) (m/z) $C_{65}H_{84}N_{20}O_7$ calcd: 1256.6832; found, 1257.7249 $[M+H]^+$,

629.3614 $[M+H]^{2+}$; **17c** c[**arg**-Arg-**arg**-Arg-**dip-trp-dip**]: HR-MS (ESI-TOF) (m/z) $C_{65}H_{84}N_{20}O_7$ calcd: 1256.6832; found, 1257.7040 $[M+H]^{+}$, 629.3614 $[M+H]^{2+}$; 419.6048 $[M+H]^{3+}$; **18c** c[Arg-**arg**-Arg-**arg-dip-trp-dip**]: HR-MS (ESI-TOF) (m/z) $C_{65}H_{84}N_{20}O_7$ calcd: 1256.6832; found, 1257.7660 $[M+H]^{+}$, 629.3620 $[M+H]^{2+}$; **19c** c[Arg-Arg-**arg-arg- dip-trp-dip**]: HR-MS (ESI-TOF) (m/z) $C_{65}H_{84}N_{20}O_7$ calcd: 1256.6832; found, 1257.7036 $[M+H]^{+}$, 629.3605 $[M+H]^{2+}$; **20c** c[**arg-arg**-Arg-Arg- **dip-trp-dip**]: HR-MS (ESI-TOF) (m/z) $C_{65}H_{84}N_{20}O_7$ calcd: 1256.6832; found, 1257.7093 $[M+H]^{+}$, 629.3629 $[M+H]^{2+}$; **21c** c[Arg-Arg-**arg-arg**-Dip-**trp**-Dip]: HR-MS (ESI-TOF) (m/z) $C_{65}H_{84}N_{20}O_7$ calcd: 1256.6832; found, 1257.9085 $[M+H]^{+}$, 629.3629 $[M+H]^{2+}$, 419.9432 $[M+H]^{3+}$; **22c** c[**arg-arg**-Arg-Arg-Dip-**trp**-Dip]: HR-MS (ESI-TOF) (m/z) $C_{65}H_{84}N_{20}O_7$ calcd: 1256.6832; found, 1257.7052 $[M+H]^{+}$, 629.3611 $[M+H]^{2+}$; 419.6057 $[M+H]^{3+}$; **23c** c[Arg-Arg-**arg-arg**-Dip-Trp-Dip]: HR-MS (ESI-TOF) (m/z) $C_{65}H_{84}N_{20}O_7$ calcd: 1256.6832; found, 1257.9030 $[M+H]^{+}$, 629.3599 $[M+H]^{2+}$; 419.9309 $[M+H]^{3+}$; **24c** c[**arg-arg**-Arg-Arg-Dip-Trp-Dip]: HR-MS (ESI-TOF) (m/z) $C_{65}H_{84}N_{20}O_7$ calcd: 1256.6832; found, 1257.9021 $[M+H]^{+}$, 629.3591 $[M+H]^{2+}$; 419.9024 $[M+H]^{3+}$;

Series 4: 1d c[Arg-Arg-Arg-Arg-Nal-Trp-**nal**]: HR-MS (ESI-TOF) (m/z) $C_{61}H_{80}N_{20}O_7$ calcd: 1204.6519; found, 1205.6746 $[M+H]^{+}$, 603.3456 $[M+H]^{2+}$; **2d** c[Arg-Arg-Arg-Arg-Nal-**trp**-Nal]: HR-MS (ESI-TOF) (m/z) $C_{61}H_{80}N_{20}O_7$ calcd: 1204.6519; found, 1205.8932 $[M+H]^{+}$, 603.3447 $[M+H]^{2+}$; **3d** c[Arg-Arg-Arg-Arg-**nal**-Trp-Nal]: HR-MS (ESI-TOF) (m/z) $C_{61}H_{80}N_{20}O_7$ calcd: 1204.6519; found, 1205.7986 $[M+H]^{+}$, 603.3449 $[M+H]^{2+}$; **4d** c[Arg-Arg-Arg-**arg**-Nal-Trp-Nal]: HR-MS (ESI-TOF) (m/z) $C_{61}H_{80}N_{20}O_7$ calcd: 1204.6519; found, 1205.6554 $[M+H]^{+}$, 603.3453 $[M+H]^{2+}$; **5d** c[Arg-Arg-**arg**-Arg-Nal-Trp-Nal]: HR-MS (ESI-TOF) (m/z) $C_{61}H_{80}N_{20}O_7$ calcd: 1204.6519; found, 1205.6730 $[M+H]^{+}$, 603.3448 $[M+H]^{2+}$; **6d** c[Arg-**arg**-Arg-Arg-Nal-Trp-Nal]: HR-MS (ESI-TOF) (m/z) $C_{61}H_{80}N_{20}O_7$ calcd: 1204.6519; found, 1205.6726 $[M+H]^{+}$, 603.3447 $[M+H]^{2+}$; **7d** c[**arg**-Arg-Arg-Arg-Nal-Trp-Nal]: HR-MS (ESI-TOF) (m/z) $C_{61}H_{80}N_{20}O_7$ calcd: 1204.6519; found, 1205.9835 $[M+H]^{+}$, 603.3429 $[M+H]^{2+}$; **8d** c[**arg-arg-arg-arg-nal-trp-nal**]: HR-MS (ESI-TOF) (m/z) $C_{61}H_{80}N_{20}O_7$ calcd: 1204.6519; found, 1205.6723 $[M+H]^{+}$, 603.3449 $[M+H]^{2+}$; **9d** c[**arg-arg-arg-arg**-Nal-Trp-Nal]: HR-MS (ESI-TOF) (m/z) $C_{61}H_{80}N_{20}O_7$ calcd: 1204.6519; found, 1205.6695 $[M+H]^{+}$, 603.3432 $[M+H]^{2+}$; **10d** c[Arg-Arg-Arg-Arg-**nal-trp-nal**]: HR-MS (ESI-TOF) (m/z) $C_{61}H_{80}N_{20}O_7$ calcd: 1204.6519; found, 1205.6711 $[M+H]^{+}$, 603.3436 $[M+H]^{2+}$; **11d** c[Arg-Arg-Arg-Arg-**nal**-Trp-**nal**]: HR-MS (ESI-TOF) (m/z) $C_{61}H_{80}N_{20}O_7$ calcd: 1204.6519; found, 1205.9972 $[M+H]^{+}$, 603.3423 $[M+H]^{2+}$; **12d** c[**arg-arg-arg-arg -nal**-Trp-**nal**]: HR-MS (ESI-

TOF) (m/z) $C_{61}H_{80}N_{20}O_7$ calcd: 1204.6519; found, 1205.8781 $[M+H]^+$, 603.3462 $[M+H]^{2+}$; **13d** c[**arg**-Arg-**arg**-Arg-**nal**-Trp-**nal**]: HR-MS (ESI-TOF) (m/z) $C_{61}H_{80}N_{20}O_7$ calcd: 1204.6519; found, 1205.6748 $[M+H]^+$, 603.3449 $[M+H]^{2+}$; **14d** c[Arg-**arg**-Arg-**arg-nal**-Trp-**nal**]: HR-MS (ESI-TOF) (m/z) $C_{61}H_{80}N_{20}O_7$ calcd: 1204.6519; found, 1205.6751 $[M+H]^+$, 603.3463 $[M+H]^{2+}$; **15d** c[Arg-Arg-**arg-arg-nal**-Trp-**nal**]: HR-MS (ESI-TOF) (m/z) $C_{61}H_{80}N_{20}O_7$ calcd: 1204.6519; found, 1205.6740 $[M+H]^+$, 603.3456 $[M+H]^{2+}$; **16d** c[**arg-arg**-Arg-Arg-**nal**-Trp-**nal**]: HR-MS (ESI-TOF) (m/z) $C_{61}H_{80}N_{20}O_7$ calcd: 1204.6519; found, 1205.6717 $[M+H]^+$, 603.3444 $[M+H]^{2+}$; **17d** c[**arg**-Arg-**arg**-Arg-**nal-trp-nal**]: HR-MS (ESI-TOF) (m/z) $C_{61}H_{80}N_{20}O_7$ calcd: 1204.6519; found, 1205.6747 $[M+H]^+$, 603.3460 $[M+H]^{2+}$; **18d** c[Arg-**arg**-Arg-**arg-nal-trp-nal**]: HR-MS (ESI-TOF) (m/z) $C_{61}H_{80}N_{20}O_7$ calcd: 1204.6519; found, 1205.6728 $[M+H]^+$, 603.3453 $[M+H]^{2+}$; **19d** c[Arg-Arg-**arg-arg-nal-trp-nal**]: HR-MS (ESI-TOF) (m/z) $C_{61}H_{80}N_{20}O_7$ calcd: 1204.6519; found, 1205.8749 $[M+H]^+$, 603.3438 $[M+H]^{2+}$; **20d** c[**arg-arg**-Arg-Arg-**nal-trp-nal**]: HR-MS (ESI-TOF) (m/z) $C_{61}H_{80}N_{20}O_7$ calcd: 1204.6519; found, 1205.9727 $[M+H]^+$, 603.3437 $[M+H]^{2+}$; **21d** c[Arg-Arg-**arg-arg**-Nal-**trp**-Nal]: HR-MS (ESI-TOF) (m/z) $C_{61}H_{80}N_{20}O_7$ calcd: 1204.6519; found, 1205.6727 $[M+H]^+$, 603.3454 $[M+H]^{2+}$; **22d** c[**arg-arg**-Arg-Arg-Nal-**trp**-Nal]: HR-MS (ESI-TOF) (m/z) $C_{61}H_{80}N_{20}O_7$ calcd: 1204.6519; found, 1205.6719 $[M+H]^+$, 603.3446 $[M+H]^{2+}$; **23d** c[Arg-Arg-**arg-arg**-Nal-Trp-Nal]: HR-MS (ESI-TOF) (m/z) $C_{61}H_{80}N_{20}O_7$ calcd: 1204.6519; found, 1205.6634 $[M+H]^+$, 603.3440 $[M+H]^{2+}$; **24d** c[**arg-arg**-Arg-Arg-Nal-Trp-Nal]: HR-MS (ESI-TOF) (m/z) $C_{61}H_{80}N_{20}O_7$ calcd: 1204.6519; found, 1205.6699 $[M+H]^+$, 603.3438 $[M+H]^{2+}$.

Series 5: 1e c[**arg-arg-arg-arg-trp-nal-nal**]: HR-MS (ESI-TOF) (m/z) $C_{61}H_{80}N_{20}O_7$ calcd: 1204.6519; found, 1205.9926 $[M+H]^+$, 603.3432 $[M+H]^{2+}$; **2e** c[**arg-arg-arg-arg**-Trp-Nal-Nal]: HR-MS (ESI-TOF) (m/z) $C_{61}H_{80}N_{20}O_7$ calcd: 1204.6519; found, 1205.6355 $[M+H]^+$, 603.3441 $[M+H]^{2+}$; **3e** c[Arg-Arg-Arg-Arg-**trp-nal-nal**]: HR-MS (ESI-TOF) (m/z) $C_{61}H_{80}N_{20}O_7$ calcd: 1204.6519; found, 1205.6739 $[M+H]^+$, 603.3457 $[M+H]^{2+}$; **4e** c[**arg**-Arg-**arg**-Arg-Trp-**nal-nal**]: HR-MS (ESI-TOF) (m/z) $C_{61}H_{80}N_{20}O_7$ calcd: 1204.6519; found, 1205.6735 $[M+H]^+$, 603.3456 $[M+H]^{2+}$; **5e** c[Arg-**arg**-Arg-**arg**-Trp-**nal-nal**]: HR-MS (ESI-TOF) (m/z) $C_{61}H_{80}N_{20}O_7$ calcd: 1204.6519; found, 1205.6742 $[M+H]^+$, 603.3457 $[M+H]^{2+}$; **6e** c[Arg-Arg-**arg-arg**-Trp-**nal-nal**]: HR-MS (ESI-TOF) (m/z) $C_{61}H_{80}N_{20}O_7$ calcd: 1204.6519; found, 1205.9540 $[M+H]^+$, 603.3461 $[M+H]^{2+}$; **7e** c[**arg-arg**-Arg-Arg-Trp-**nal-nal**]: HR-MS (ESI-TOF) (m/z) $C_{61}H_{80}N_{20}O_7$ calcd: 1204.6519; found, 1205.6760 $[M+H]^+$, 603.3474 $[M+H]^{2+}$; **8e** c[Arg-Arg-**arg-arg-trp-nal-nal**]: HR-MS (ESI-TOF) (m/z) $C_{61}H_{80}N_{20}O_7$ calcd:

1204.6519; found, 1205.6754 $[M+H]^+$, 603.3475 $[M+H]^{2+}$; **9e** c[**arg-arg**-Arg-Arg-**trp-nal-nal**]: HR-MS (ESI-TOF) (m/z) $C_{61}H_{80}N_{20}O_7$ calcd: 1204.6519; found, 1205.6741 $[M+H]^+$, 603.3472 $[M+H]^{2+}$; **10e** c[Arg-Arg-**arg-arg-trp**-Nal-Nal]: HR-MS (ESI-TOF) (m/z) $C_{61}H_{80}N_{20}O_7$ calcd: 1204.6519; found, 1205.6720 $[M+H]^+$, 603.3452 $[M+H]^{2+}$; **11e** c[**arg-arg**-Arg-Arg-**trp**-Nal-Nal]: HR-MS (ESI-TOF) (m/z) $C_{61}H_{80}N_{20}O_7$ calcd: 1204.6519; found, 1205.7486 $[M+H]^+$, 603.4934 $[M+H]^{2+}$.

4.4. Measurement of antibacterial activity

The antibacterial activity of all the synthesized cyclic peptides was evaluated by screening them against a variety of susceptible and drug-resistant bacterial strains. Antibacterial susceptibility testing was conducted using a standard microtiter dilution method, as recommended by the Clinical and Laboratory Standard Institute (CLSI) and measured as the minimum inhibitory concentration (MIC). The MIC is defined as the lowest peptide concentration required to inhibit bacterial growth. A detailed description of the bacterial strains and their growth conditions is provided in the supplementary information (Table S1). Briefly, the bacterial cells were cultured overnight at 37 ºC in the appropriate broth for each strain, then diluted in cation-adjusted Mueller Hinton Broth (CAMHB). Serial dilutions of the peptides were added to the microtiter plates in a 100 µL volume, followed by the addition of 100 µL of bacterial suspension, achieving a final inoculum of 5×10^5 colony forming units (CFU)/mL. The plates were incubated at 37 ºC for 24 h, and the MICs were determined. All experiments were performed in triplicate.

4.5. Measurement of antifungal activity

The MICs of all the synthesized cyclic peptides against fungal strains (*A. fumigatus*, *C. albicans*, and *C. krusii*) was determined using the microscale broth dilution method, as outlined by the M27-A3 documents of the Clinical and Laboratory Standard Institute (CLSI).[35] Briefly, planktonic cells cultured in Sabouraud dextrose Broth (SDB) were harvested at mid-logarithmic phase, washed with 10 mM phosphate-buffered saline (PBS, pH 7.4), and re-suspended at a density of 0.5~2.5 × 10^3 CFU/mL in RPMI 1640 medium (Gibco, BRL Invitrogen, US). A 100 µL portion of the fungal suspension and 100 µL of each peptide (with final concentrations ranging from 0.7-100 µg/mL) and standard antibiotics (Amphotericin B and Fluconazole) were added to a 96-well plate for susceptibility testing. The plates were incubated at 35 °C for 48 h (*Candida* strains) and 72 h (*Aspergillus* strain). The OD at 630 nm for each well was measured using a microplate reader. The lowest concentration corresponding

to no visible fungal growth, compared to the negative control was considered as the MIC. The assays were conducted in triplicate, with each experiment replicated twice.

4.6. Antibiofilm activity

The anti-biofilm potential of lead peptides **15c** and **16c** was evaluated against pre-formed biofilm of bacteria (MRSA and *E. coli*) and fungi (*A. fumigatus* and *C. albicans*) as described previously with some modifications.[36] Briefly, bacterial cell suspensions were adjusted to 5×10^5 CFU/mL in Mueller-Hinton (MH) broth and plated into 96-well polystyrene microtiter plates, followed by incubation at 37 °C for 24 h. Similarly, fungal suspensions were adjusted to 2×10^7 CFU/mL in RPMI medium, and 100 µL of these suspensions were added to 96-well polystyrene microtiter plates, then incubated at 35 °C for 24 h. After incubation, both bacterial and fungal biofilms were gently washed twice with phosphate-buffered saline (PBS). A 100 µL of test peptides or standard antibiotics at their MIC and 2×MIC concentrations were added into the wells of pre-washed biofilms, and the plates were incubated at 37 °C (for bacterial biofilms) and 35 °C (for fungal biofilms) for 24 h.

Subsequently, the reduction in the biofilm burden was determined using 2,3-Bis-(2-Methoxy-4-Nitro-5-Sulfophenyl)-2H-Tetrazolium-5-Carboxanilide (XTT) and phenazine methosulfate. Stock solutions of XTT (1 mg/mL) and phenazine methosulfate (0.32 mg/mL) were prepared in PBS and water, respectively, and stored away from light. After drug dilutions were removed from each well, the biofilms were gently washed twice with PBS. To each well, 90 µL XTT and 10 µL phenazine methosulfate were added. The plates were incubated in the dark at 37 °C for 1 h, and the absorbance at 492 nm was recorded using an automated plate reader. The experiment was performed in triplicate and repeated twice.

4.7. Measurement of hemolytic activity

The hemolytic activity of the peptides was evaluated using human red blood cells (hRBC) purchased from BioIVT, USA. The hRBCs were centrifuged for 15 min to remove the buffy coat and washed three times with phosphate buffer saline (100 mM NaCl, 80 mM Na_2HPO_4, 20 mM NaH_2PO_4, pH 7.4). Hemolysis induced by the peptides was tested in triplicate by mixing 75 µL of peptide solution (prepared through two-fold serial dilution) with 75 µL of a 4 % (v/v) hRBC suspension in PBS. The plates were incubated for 2 h at 37 °C without agitation, then centrifuged at 1000 g for 10 min. Aliquots (100 µL) of the supernatant were transferred to 96-well plates, and hemoglobin release was measured spectrophotometrically at 567 nm. The percentage of hemolysis was calculated by the following formula:

$$\text{Percentage hemolysis} = 100 \times [(A - A_0)/(A_t - A_0)]$$

Where, A represents the absorbance of the peptide sample at 567 nm, A_0 and A_t represent zero percent and 100% hemolysis determined in PBS and 1% Triton X-100, respectively.

4.8. Cytotoxicity

The *in vitro* cytotoxicity of the lead cyclic peptides from Series 1 (**7a** and **12a**), Series 2 (**7b** and **12b**), Series 3 (**15c**, **16c**, and **20c**), Series 4 (**15d** and **16d**), and their respective parent peptides (**p1**, **p2**, **p3**, and **p4**) was examined using human lung fibroblast cell (MRC-5), human embryonic kidney cells (HEK-293), human liver cells (HPRGC10), and human skin fibroblast cells (HeKa). The cells were seeded at 10,000 per well in 0.1 mL media in 96 well plates 24 h prior to the experiment. Lung and kidney cells were seeded in DMEM medium supplemented with FBS (10%). Liver cells were seeded in William's E medium with GlutaMAX supplement. The peptides were added to each well in triplicates at a variable concentration of 12.5-250 μg/mL and incubated for 24 h at 37 °C in a humidified atmosphere of 5% CO_2. After the incubation period, MTS solution (20 μL) was added to each well. Then the cells were incubated for 2 h at 37 °C. Cell viability was determined by measuring the absorbance at 490 nm using a SpectraMaxM2 microplate spectrophotometer. The percentage of cell survival was calculated as [(OD value of cells treated with the test mixture of compounds)−(OD value of culture medium)]/[(OD value of control cells)−(OD value of culture medium)]× 100%.

4.9. Kill kinetics assay

The time course of bacterial killing was studied by exposing overnight grown cultures of MRSA (ATCC BAA-1556) and *E. coli* (ATCC BAA-2452) to lead cyclic peptides (**15c** and **16c**) at their MIC and 4×MIC in MHB media as described previously.[37] Aliquots (50 μL) were drawn at a fixed time interval and plated after dilution (up to 10^8) and plated onto on MH agar plates. Viable colonies (CFU) were counted after 24 h incubation at 37 °C. Untreated bacterial culture was used as a control. The bactericidal kinetics of the standard antibiotics daptomycin, polymyxin B, and ciprofloxacin were also determined at their respective MIC and 4×MIC concentrations.

Similarly, overnight grown cultures of *A. fumigatus* and *C. albicans* were used to prepare fungal suspensions, which then adjusted to approximately ~10^5 CFU/mL in sterile RPMI 1640 medium. Upon treatment with test compounds, aliquots (50 μL) were removed at a fixed time intervals and inoculated on Sabouraud dextrose agar (SDA) plates at specific times. CFU were counted after 48 h incubation at 35°C. Fluconazole and Amphotericin B were used as positive controls. The assays were conducted in triplicate, with each experiment replicated twice.

4.10. Calcein dye leakage assay

The calcein dye leakage assay was conducted by using calcein dye encapsulated large unilamellar vesicles (LUVs) prepared according to a previously described protocol.[30] Peptide-induced leakage of calcein from the LUVs was monitored by measuring the fluorescence intensity at an excitation wavelength of 490 nm and an emission wavelength of 520 nm on a SpectraMax M5 multi-mode microplate reader. To achieve a final lipid concentration of 40 µM, the liposome suspension was diluted in PBS. The assay was conducted in triplicate by mixing 50 µL of peptide solution at various concentrations (5, 10, 20, 30, and 50 µg/mL) with 50 µL of liposome suspension. Calcein release from LUVs was assessed for 100 min and the measurement was taken at the interval of 10 min. The fluorescence intensity corresponding to 100% calcein release was determined by the addition of a 10% solution (w/v) of Triton X-100. The apparent percentage of dye leakage was calculated using the following formula:

$$\% \text{ Dye leakage} = 100 \times [(F - F_0)/ (F_t - F_0)]$$

Where F is the intensity measured at a given concentration of peptide, F_0 is the intensity of the liposomes (background), and F_t is the intensity after lysis induced by Triton X-100.

4.11. SEM analysis

Overnight grown bacterial culture of MRSA (ATCC BAA-1556) and *E. coli* (ATCC BAA-2452) were suspended at 10^7 CFU/mL in 10 mM PBS (pH 7.4). Aliquots of 250 µL of bacterial suspension were mixed with 30 µL test peptides (**15c** and **16c**) at final concentrations of MIC and 4×MIC and incubated at 37 °C for 30 min. Controls were run without the peptides. After 30 min incubation, the cells were fixed with an equal volume of 4% glutaraldehyde in 0.2 M Na-cacodylate buffer, pH 7.4, for 3 h at 4 °C, followed by dehydration with a graded series of ethanol and dried the sample using HMDS (hexamethyl disilazane). Coating with a 20 nm thick layer of Au/Pd was applied, and the samples were examines under a scanning electron microscope (Zeiss Sigma 300).

4.12. NMR Spectroscopy

NMR spectra were recorded on a Bruker Ascend spectrometer (400 MHz) equipped with a Prodigy Broadband (BBI) Cryoprobe. All NMR data were acquired and processed using Topspin software (Bruker). All NMR spectra were recorded using standard Bruker pulse sequences with gradient water suppression. For evaluation of peptide oligomerization, ^{1}H-NMR spectra were measured in water solution at different peptide concentrations (1.5, 0.5, 0.3, and 0.15 mM) at 25 ºC and changes in the linewidths and accessibility of the backbone amide resonances to water were analyzed using 1D and 2D ^{1}H-NMR. For the analysis of the interaction with liposomes the peptides were mixed with different amounts of DOPC/DOPG

(7:3 lipid ratio) or DOPC/Cholesterol (ratio 9:1) liposomes prepared, as described above. The final concentration of the peptides was 1.5 mM and lipid:peptide molar ratio in the samples was 1:4.35. The peptide-liposome mixtures were analyzed using both 1D and 2D ^{1}H-NMR.

4.13. MD simulations and data analysis

To probe the conformational properties of a number of D-isomers (**5a**, **7a**, **8a**, **8c**, **13c**, **15c** and **16c**) of parent cyclic peptides **p1** and **p3**, a series of all-atom MD simulations were performed in an aqueous solution. The initial spatial structures of the peptides were constructed with Maestro version 9.3.5. A number of independent MD runs, each lasting 500 ns, were conducted for each peptide, resulting in a cumulative simulation time of 2.0 μs (for **8a**, **8c** and **15c**) and 4.0 μs (for **5a**, **7a**, **13c**, **16c**). The topology for the non-standard amino acid residue (Dip) had been previously generated[30] using a set of CHARMM36 force field parameters. The preparation and production stages of the MD process were consistent for all peptides and were described previously.[30] In all calculations, the tip3p[38] water model and 3D periodic boundary conditions were employed. To maintain the system electrically neutral, Cl counterions were introduced. A spherical cutoff function (12 Å) and the particle mesh Ewald (PME) algorithm[39] (with a 12 Å cutoff) were used to treat van der Waals and electrostatic interactions, respectively. To enhance the conformational sampling, the constructed peptides were simulated at temperatures of 310 and 325 K. MD production runs (a half of runs at 325 K) were conducted in an NPT ensemble with an integration step of 2 fs.

All-atom MD simulations of the peptides, parent p8C and less cytotoxic **7a**, in a water-membrane environments were performed. The model membrane mimicking the mammalian cells was represented by a DOPC lipid bilayer. In addition, MD simulation of peptide **7a** was carried out in the presence of a two-component bilayer (DOPC/DOPG with a molar ratio of 75/25%) mimicking a bacterial membrane. The MD data obtained were compared with the results of modeling of **p1** in an analogous water-bilayer system, described earlier[30]. Both model membranes contained 128 lipid molecules. Finally, multiple MD production runs were conducted in an *NPT* ensemble at a semi-isotropic pressure and a constant temperature of 310 K with an integration step of 2 fs.

For each peptide, three starting conformations were selected. Two of the which represent the most populated clusters of the water MD states, determined using RMSD-based clustering algorithm. The third conformation was the initial spatial model used as starting one in MD simulations in water. For each starting conformation of the peptides, MD calculations (with a duration of 200 ns) were conducted starting from 4 varied orientations, so that the

different sides of the peptide molecules were facing the membrane. The GROMACS[40] package version 2020.4 and the all-atom CHARMM36[41] force field were used for all MD simulations. *Data analysis*. MD data were analyzed and averaged over all sets of MD trajectories. MD-trajectories of the original peptides (**p1** and **p3** used for the analysis have been obtained previously.[30, 32] MD trajectories were sampled for analysis at time intervals of 1000 ps. Conformational mobility and hydrogen bonds of the peptides were evaluated using standard GROMACS utilities (gmx rms, gmx hbond, gmx cluster). The solvent-accessible surface areas (ASA) of the whole peptide and its polar backbone as well as the ASA named as "contact area" of the peptide that is in contact with membrane lipids were calculated by naccess v. 2.1.1 software.[42] The inter and intramolecular contacts, including stacking/pi-interactions and hydrogen bonds, as well as dihedral angle distributions were done using original in-house software utilities. The depth of peptide insertion into the membrane was delineated using GROMACS tools (*gmx distance*) and in-house software utilities.

The distribution of hydrophobic/hydrophilic properties on the molecular surfaces of peptides was calculated using the MHP approach[43], implemented in the freely available PLATINUM software.[44] For the analysis, MHP values were calculated in log P units, where P is the octanol water distribution coefficient. Mapping the time-averaged hydrophobic properties of the peptides' surfaces was done employing the Protein Surface Topography technique[45] and original in-house software. Molecular graphics were rendered using PyMOL v. 2.5 (http://pymol.org).

Funding: This project was supported by NIH Grant 1R41AI164997-01A1 and funds from Dr. Assad Kazeminy, AJK Biopharmaceutical, and Chapman University (KP). Molecular modeling work was supported by the Ministry of Science and Higher Education of the Russian Federation (Agreement No. 075-15-2020-773).

Acknowledgments: The authors acknowledge the support of the core facility at Chapman University School of Pharmacy. We gratefully thank the computational facilities of the Supercomputer Center "Polytechnical" at the St. Petersburg Polytechnic University for providing access. We acknowledge the National Institute of Health for subcontracting testing of a number of compounds against additional ESKAPE pathogens and fungi, as shown in Tables 1 and 2.

Data Availability Statement: The data supporting this article have been included as part of the Supplementary Information.

Author Contributions

K.P., R.T., and S.L. planned and designed the experiments; S.L. performed the chemistry and antimicrobial, cytotoxicity work, and mechanistic studies; E.J.M.M and N.H.H. conducted antibacterial and antifungal assays; I.M. and S.K.J. conducted the NMR studies; A.K. and R.E. performed the simulation studies; K.P. and R.T. contributed reagents/materials/analysis tools; S.L., K.P., I.M., A.K, and R.E. wrote the manuscript. All authors have read and agreed to the published version of the manuscript.

Conflicts of Interest: The authors declare no conflict of interest.

References:

1. M. E. de Kraker, A. J. Stewardson and S. Harbarth, Will 10 million people die a year due to antimicrobial resistance by 2050?, *PLoS medicine*, 2016, **13**, e1002184.
2. C. L. Ventola, The antibiotic resistance crisis: part 1: causes and threats, *Pharmacy and therapeutics*, 2015, **40**, 277.
3. X. Zhen, C. S. Lundborg, X. Sun, X. Hu and H. Dong, Economic burden of antibiotic resistance in ESKAPE organisms: a systematic review, *Antimicrobial Resistance & Infection Control*, 2019, **8**, 1-23.
4. R. R. Roberts, B. Hota, I. Ahmad, R. D. Scott, S. D. Foster, F. Abbasi, S. Schabowski, L. M. Kampe, G. G. Ciavarella and M. Supino, Hospital and societal costs of antimicrobial-resistant infections in a Chicago teaching hospital: implications for antibiotic stewardship, *Clinical infectious diseases*, 2009, **49**, 1175-1184.
5. R. Hancock and A. Patrzykat, Clinical development of cationic antimicrobial peptides: from natural to novel antibiotics, *Current drug targets-Infectious disorders*, 2002, **2**, 79-83.
6. H.-Y. Yi, M. Chowdhury, Y.-D. Huang and X.-Q. Yu, Insect antimicrobial peptides and their applications, *Applied microbiology and biotechnology*, 2014, **98**, 5807-5822.
7. N. Boulanger, R. Brun, L. Ehret-Sabatier, C. Kunz and P. Bulet, Immunopeptides in the defense reactions of Glossina morsitans to bacterial and Trypanosoma brucei brucei infections, *Insect biochemistry and molecular biology*, 2002, **32**, 369-375.
8. J. Lei, L. Sun, S. Huang, C. Zhu, P. Li, J. He, V. Mackey, D. H. Coy and Q. He, The antimicrobial peptides and their potential clinical applications, *American journal of translational research*, 2019, **11**, 3919.
9. M. Mahlapuu, J. Håkansson, L. Ringstad and C. Björn, Antimicrobial peptides: an emerging category of therapeutic agents, *Frontiers in cellular and infection microbiology*, 2016, 194.
10. T. Rončević, J. Puizina and A. Tossi, Antimicrobial peptides as anti-infective agents in pre-post-antibiotic era?, *International journal of molecular sciences*, 2019, **20**, 5713.
11. Y. Shai, Mode of action of membrane active antimicrobial peptides, *Peptide Science: Original Research on Biomolecules*, 2002, **66**, 236-248.

12. G. G. Perron, M. Zasloff and G. Bell, Experimental evolution of resistance to an antimicrobial peptide, *Proceedings of the Royal Society B: Biological Sciences*, 2006, **273**, 251-256.
13. C. Weidenmaier, S. A. Kristian and A. Peschel, Bacterial resistance to antimicrobial host defenses-an emerging target for novel antiinfective strategies?, *Current drug targets*, 2003, **4**, 643-649.
14. J. D. Hale and R. E. Hancock, Alternative mechanisms of action of cationic antimicrobial peptides on bacteria, *Expert review of anti-infective therapy*, 2007, **5**, 951-959.
15. C.-F. Le, C.-M. Fang and S. D. Sekaran, Intracellular targeting mechanisms by antimicrobial peptides, *Antimicrobial agents and chemotherapy*, 2017, **61**, 10.1128/aac. 02340-02316.
16. J. M. Sierra, E. Fusté, F. Rabanal, T. Vinuesa and M. Viñas, An overview of antimicrobial peptides and the latest advances in their development, *Expert opinion on biological therapy*, 2017, **17**, 663-676.
17. K. E Greber and M. Dawgul, Antimicrobial peptides under clinical trials, *Current topics in medicinal chemistry*, 2017, **17**, 620-628.
18. L. Czaplewski, R. Bax, M. Clokie, M. Dawson, H. Fairhead, V. A. Fischetti, S. Foster, B. F. Gilmore, R. E. Hancock and D. Harper, Alternatives to antibiotics—a pipeline portfolio review, *The Lancet infectious diseases*, 2016, **16**, 239-251.
19. S. Ramesh, T. Govender, H. G. Kruger, B. G. de la Torre and F. Albericio, Short AntiMicrobial Peptides (SAMPs) as a class of extraordinary promising therapeutic agents, *Journal of Peptide Science*, 2016, **22**, 438-451.
20. G. S. Dijksteel, M. M. Ulrich, E. Middelkoop and B. K. Boekema, Lessons learned from clinical trials using antimicrobial peptides (AMPs), *Frontiers in microbiology*, 2021, **12**, 616979.
21. L. You, R. An, K. Liang, B. Cui and X. Wang, Macrocyclic compounds: emerging opportunities for current drug discovery, *Current Pharmaceutical Design*, 2016, **22**, 4086-4093.
22. D. Garcia Jimenez, V. Poongavanam and J. Kihlberg, Macrocycles in Drug Discovery– Learning from the Past for the Future, *Journal of Medicinal Chemistry*, 2023, **66**, 5377-5396.
23. Y. Huang, M. M. Wiedmann and H. Suga, RNA display methods for the discovery of bioactive macrocycles, *Chemical reviews*, 2018, **119**, 10360-10391.
24. A. Bin Hafeez, X. Jiang, P. J. Bergen and Y. Zhu, Antimicrobial peptides: An update on classifications and databases, *International journal of molecular sciences*, 2021, **22**, 11691.
25. D. L. Lee and R. S. Hodges, Structure–activity relationships of de novo designed cyclic antimicrobial peptides based on gramicidin S, *Peptide Science*, 2003, **71**, 28-48.
26. J. Zhang, Y. Zhao, S. Han, C. Chen and H. Xu, Self-assembly of surfactant-like peptides and their applications, *Science China Chemistry*, 2014, **57**, 1634-1645.
27. M. Pirtskhalava, B. Vishnepolsky, M. Grigolava and G. Managadze, Physicochemical Features and Peculiarities of Interaction of AMP with the Membrane, *Pharmaceuticals*, 2021, **14**, 471.
28. S. Lohan, A. G. Konshina, R. G. Efremov, I. Maslennikov and K. Parang, Structure-Based Rational Design of Small α-Helical Peptides with Broad-Spectrum Activity against Multidrug-Resistant Pathogens, *Journal of Medicinal Chemistry*, 2022, **66**, 855-874.
29. E. H. Mohammed, S. Lohan, T. Ghaffari, S. Gupta, R. K. Tiwari and K. Parang, Membrane-Active Cyclic Amphiphilic Peptides: Broad-Spectrum Antibacterial Activity Alone and in Combination with Antibiotics, *Journal of Medicinal Chemistry*, 2022, **65**, 15819-15839.
30. S. Lohan, D. Mandal, W. Choi, A. G. Konshina, R. K. Tiwari, R. G. Efremov, I. Maslennikov and K. Parang, Small amphiphilic peptides: activity against a broad range of drug-resistant bacteria and structural insight into membranolytic properties, *Journal of Medicinal Chemistry*, 2022, **65**, 665-687.
31. E. H. Mohammed, S. Lohan, R. K. Tiwari and K. Parang, Amphiphilic cyclic peptide [W4KR5]-Antibiotics combinations as broad-spectrum antimicrobial agents, *European Journal of Medicinal Chemistry*, 2022, **235**, 114278.

32. S. Lohan, A. G. Konshina, R. K. Tiwari, R. G. Efremov, I. Maslennikov and K. Parang, Broad-spectrum activity of membranolytic cationic macrocyclic peptides against multi-drug resistant bacteria and fungi, *European Journal of Pharmaceutical Sciences*, 2024, **197**, 106776.
33. E. M. Molhoek, A. Van Dijk, E. J. Veldhuizen, H. P. Haagsman and F. J. Bikker, Improved proteolytic stability of chicken cathelicidin-2 derived peptides by D-amino acid substitutions and cyclization, *Peptides*, 2011, **32**, 875-880.
34. S. A. El-Mowafi, A. G. Konshina, E. H. Mohammed, N. A. Krylov, R. G. Efremov and K. Parang, Structural Analysis and Activity Correlation of Amphiphilic Cyclic Antimicrobial Peptides Derived from the [W4R4] Scaffold, *Molecules*, 2023, **28**, 8049.
35. W. PA, Reference method for broth dilution antifungal susceptibility testing of yeasts, Approved standard, *CLSI document M27-A2*, 2002.
36. A. Di Somma, A. Moretta, C. Canè, A. Cirillo and A. Duilio, Antimicrobial and antibiofilm peptides, *Biomolecules*, 2020, **10**, 652.
37. F. H. Waghu, S. Joseph, S. Ghawali, E. A. Martis, T. Madan, K. V. Venkatesh and S. Idicula-Thomas, Designing antibacterial peptides with enhanced killing kinetics, *Frontiers in Microbiology*, 2018, **9**, 325.
38. W. L. Jorgensen and J. Tirado-Rives, Potential energy functions for atomic-level simulations of water and organic and biomolecular systems, *Proceedings of the National Academy of Sciences*, 2005, **102**, 6665-6670.
39. U. Essmann, L. Perera, M. L. Berkowitz, T. Darden, H. Lee and L. G. Pedersen, A smooth particle mesh Ewald method, *The Journal of chemical physics*, 1995, **103**, 8577-8593.
40. M. J. Abraham, T. Murtola, R. Schulz, S. Páll, J. C. Smith, B. Hess and E. Lindahl, GROMACS: High performance molecular simulations through multi-level parallelism from laptops to supercomputers, *SoftwareX*, 2015, **1**, 19-25.
41. J. B. Klauda, R. M. Venable, J. A. Freites, J. W. O'Connor, D. J. Tobias, C. Mondragon-Ramirez, I. Vorobyov, A. D. MacKerell Jr and R. W. Pastor, Update of the CHARMM all-atom additive force field for lipids: validation on six lipid types, *The journal of physical chemistry B*, 2010, **114**, 7830-7843.
42. S. Hubbard and J. Thornton, Naccess: Department of biochemistry and molecular biology, university college london, *Software available at http://www.bioinf.manchester.ac.uk/naccess/nacdownload.html*, 1993.
43. R. G. Efremov and A. J. Alix, Environmental characteristics of residues in proteins: three-dimensional molecular hydrophobicity potential approach, *Journal of Biomolecular Structure and Dynamics*, 1993, **11**, 483-507.
44. T. V. Pyrkov, A. O. Chugunov, N. A. Krylov, D. E. Nolde and R. G. Efremov, PLATINUM: a web tool for analysis of hydrophobic/hydrophilic organization of biomolecular complexes, *Bioinformatics*, 2009, **25**, 1201-1202.
45. A. D. Koromyslova, A. O. Chugunov and R. G. Efremov, Deciphering fine molecular details of proteins' structure and function with a protein surface topography (pst) method, *Journal of chemical information and modeling*, 2014, **54**, 1189-1199.